



This is a repository copy of *Kinetic and structural characterization of NUDT15 and NUDT18 as catalysts of isoprene pyrophosphate hydrolysis*.

White Rose Research Online URL for this paper:

<https://eprints.whiterose.ac.uk/215617/>

Version: Published Version

---

**Article:**

Scaletti, E.R., Unterlass, J.E., Almlöf, I. et al. (7 more authors) (2024) Kinetic and structural characterization of NUDT15 and NUDT18 as catalysts of isoprene pyrophosphate hydrolysis. *The FEBS Journal*, 291 (19). pp. 4301-4322. ISSN 1742-464X

<https://doi.org/10.1111/febs.17202>

---

**Reuse**

This article is distributed under the terms of the Creative Commons Attribution (CC BY) licence. This licence allows you to distribute, remix, tweak, and build upon the work, even commercially, as long as you credit the authors for the original work. More information and the full terms of the licence here:

<https://creativecommons.org/licenses/>




**Takedown**

If you consider content in White Rose Research Online to be in breach of UK law, please notify us by emailing [eprints@whiterose.ac.uk](mailto:eprints@whiterose.ac.uk) including the URL of the record and the reason for the withdrawal request.



[eprints@whiterose.ac.uk](mailto:eprints@whiterose.ac.uk)  
<https://eprints.whiterose.ac.uk/>

# Kinetic and structural characterization of NUDT15 and NUDT18 as catalysts of isoprene pyrophosphate hydrolysis

Emma R. Scaletti<sup>1</sup>, Judith E. Unterlass<sup>2</sup>, Ingrid Almlöf<sup>2</sup>, Tobias Koolmeister<sup>2</sup>, Karl S. Vallin<sup>2</sup>, Despina Kapsitidou<sup>2</sup>, Viktoriia Tsuber<sup>2</sup>, Thomas Helleday<sup>2</sup> , Pål Stenmark<sup>1</sup>  and Ann-Sofie Jemth<sup>2</sup> 

<sup>1</sup> Department of Biochemistry and Biophysics, Stockholm University, Sweden

<sup>2</sup> Department of Oncology-Pathology, Science for Life Laboratory, Karolinska Institutet, Stockholm, 171 77, Sweden

## Keywords

enzyme catalysis; hydrolysis; isoprene pyrophosphate; NUDT15; NUDT18

## Correspondence

A.-S. Jemth, Department of Oncology-Pathology, Science for Life Laboratory, Karolinska Institutet, Stockholm 171 77, Sweden

Tel: +46-768292927

E-mail: [ann-sofie.jemth@ki.se](mailto:ann-sofie.jemth@ki.se)

and

P. Stenmark, Department of Biochemistry and Biophysics, Stockholm University, Stockholm 106 91, Sweden

Tel: +46-8163729

E-mail: [stenmark@dbb.su.se](mailto:stenmark@dbb.su.se)

(Received 12 January 2024, revised 19 April 2024, accepted 6 June 2024)

doi:10.1111/febs.17202

Isoprene pyrophosphates play a crucial role in the synthesis of a diverse array of essential nonsterol and sterol biomolecules and serve as substrates for posttranslational isoprenylation of proteins, enabling specific anchoring to cellular membranes. Hydrolysis of isoprene pyrophosphates would be a means to modulate their levels, downstream products, and protein isoprenylation. While NUDIX hydrolases from plants have been described to catalyze the hydrolysis of isoprene pyrophosphates, homologous enzymes with this function in animals have not yet been reported. In this study, we screened an extensive panel of human NUDIX hydrolases for activity in hydrolyzing isoprene pyrophosphates. We found that human nucleotide triphosphate diphosphatase NUDT15 and 8-oxo-dGDP phosphatase NUDT18 efficiently catalyze the hydrolysis of several physiologically relevant isoprene pyrophosphates. Notably, we demonstrate that geranyl pyrophosphate is an excellent substrate for NUDT18, with a catalytic efficiency of  $2.1 \times 10^5 \text{ M}^{-1} \cdot \text{s}^{-1}$ , thus making it the best substrate identified for NUDT18 to date. Similarly, geranyl pyrophosphate proved to be the best isoprene pyrophosphate substrate for NUDT15, with a catalytic efficiency of  $4.0 \times 10^4 \text{ M}^{-1} \cdot \text{s}^{-1}$ . LC-MS analysis of NUDT15 and NUDT18 catalyzed isoprene pyrophosphate hydrolysis revealed the generation of the corresponding monophosphates and inorganic phosphate. Furthermore, we solved the crystal structure of NUDT15 in complex with the hydrolysis product geranyl phosphate at a resolution of 1.70 Å. This structure revealed that the active site nicely accommodates the hydrophobic isoprenoid moiety and helped identify key binding residues. Our findings imply that isoprene pyrophosphates are endogenous substrates of NUDT15 and NUDT18, suggesting they are involved in animal isoprene pyrophosphate metabolism.

## Abbreviations

8-oxo-dGDP, 8-oxo-2'-deoxyguanosine-5'-diphosphate; AtNUDT1, *Arabidopsis thaliana* NUDIX hydrolase 1; dGTP, deoxyguanosine-5'-triphosphate; DMAPP, dimethylallyl pyrophosphate; FOH, farnesol; FP, farnesyl monophosphate; FPP, farnesyl pyrophosphate; FPPS, farnesyl pyrophosphate synthase; GGOH, geranylgeraniol; GGPP, geranylgeranyl pyrophosphate; GGPPS, geranylgeranyl pyrophosphate synthase; GOH, geraniol; GP, geranyl monophosphate; GPP, geranyl pyrophosphate; HMG-CoA reductase, 3-hydroxy-3-methylglutaryl-CoA reductase; IPPP, isopentenyl pyrophosphate; IPTG, isopropyl β-D-1-thiogalactopyranoside; MK, mevalonate kinase; MPP, mevalonate pyrophosphate; NUDIX, nucleoside diphosphates linked to a number of different moieties (x); NUDT15, NUDIX hydrolase 15; NUDT18, NUDIX hydrolase 18; Pi, inorganic phosphate; PP, pyrophosphate; PPase, pyrophosphatase; PPI, inorganic pyrophosphate; TCEP, tris(2-carboxyethyl)phosphine.

## Introduction

Isoprene pyrophosphates (isoprene PPs) are metabolites in the mevalonate pathway which is an essential metabolic pathway found in eukaryotes, archaea, and some prokaryotes [1] and is responsible for the multi-step conversion of acetyl-CoA into isopentenyl pyrophosphate (IPPP) and its isomer dimethylallyl pyrophosphate (DMAPP). IPPP and DMAPP are used as building blocks in the biosynthesis of all mammalian isoprenoids. In addition, IPPP and DMAPP are used to produce a diverse array of essential nonsterol and sterol biomolecules. An example is cholesterol which is crucial for maintaining cell membrane integrity and used for the production of steroid hormones and bile acids. Other products derived from isoprene PPs are lipoproteins, vitamin K, heme A, the mitochondrial electron carrier ubiquinone, dolichol, and isopentenyladenine used in tRNA modification [1,2]. Consequently, the isoprene PPs produced by the mevalonate pathway are crucial for a plethora of important biological processes. Figure 1 shows the chemical structures of the physiologically relevant isoprene pyrophosphates (isoprene PPs) in animals.

Moreover, approximately 2% of all mammalian proteins undergo posttranslational isoprenylation [3]. This process involves the covalent attachment of hydrophobic C-15 isoprene farnesyl or the C-20 isoprene geranylgeranyl group to cysteine residues in the C-terminal end of various proteins. Proteins that are farnesylated include the small GTP-binding proteins (GTPases) exemplified by the Ras superfamily, whereas other small GTPases such as Rab and Rho GTPases are geranylgeranylated [4]. Prenylation of proteins enables their attachment to cellular membranes, a prerequisite for these proteins to exert their specific functions in biological processes such as cell survival, cell signaling, and proliferation [5].

The dysregulation of isoprenoid biosynthesis has been implicated in several biochemical disorders, underscoring the crucial role of appropriate isoprenoid levels in maintaining proper cellular function [6–8]. Additionally, statins, commonly employed to reduce cholesterol levels, exhibit effects beyond cholesterol regulation likely mediated by changes in isoprene metabolite levels [9]. These statin-induced alterations impact fundamental processes such as cell cycle regulation, cell migration, cell proliferation, and cell survival [7,10]. Given the significance of isoprenoid metabolites, their levels are presumably tightly controlled. Indeed, mevalonate kinase (MK), the second enzyme in the isoprene biosynthesis pathway, is subject to feedback inhibition by intermediates of the isoprenoid pathway—geranyl pyrophosphate (GPP), farnesyl pyrophosphate (FPP), and geranylgeranyl pyrophosphate (GGPP) [11]. Furthermore, HMG-CoA reductase, which catalyzes the rate-limiting step in sterol and isoprenoid biosynthesis, is regulated through a feedback loop to maintain cholesterol levels within appropriate ranges while nonsterol isoprenoids are still being produced. Sterol molecules and geranylgeraniol (GGOH) participate in this feedback loop by promoting the proteasomal breakdown of the HMG-CoA reductase enzyme [12]. In addition, geraniol (GOH) and farnesol (FOH) have been demonstrated to have inhibitory effects on HMG-CoA reductase activity [13–16]. How these isoprenoid alcohols are produced in human cells remains unclear, however, a membrane-bound polyisoprenoid diphosphate phosphatase (PDP1) has been suggested to be involved in this process [17,18]. However, no cytosolic phosphatases capable of catalyzing the hydrolysis of isoprene pyrophosphates have been identified to date. NUDIX hydrolases constitute a superfamily of enzymes that catalyze the hydrolysis of a

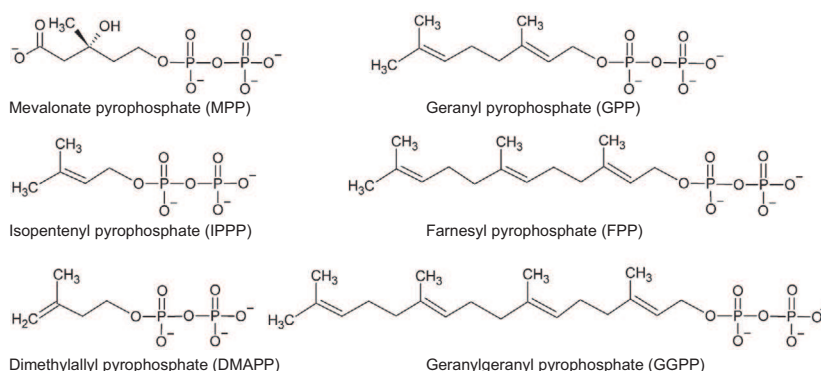


**Fig. 1.** Chemical structures of physiologically relevant isoprene-PPs. Abbreviations used in the article are shown within parentheses.

wide range of organic pyrophosphates including canonical and oxidized (d)NTPs, non-nucleoside polyphosphates, capped mRNAs, and NDP-sugars [19,20]. NUDIX hydrolases are found across different types of organisms including eukaryotes, bacteria, and archaea, and have diverse functions, including roles in RNA processing, DNA repair, and cellular metabolism [21].

Inspired by the finding that NUDIX enzymes in the plants *Arabidopsis thaliana* (mouse-ear cress) and *Rosa hybrid cultivar* (rose) can convert GPP to Geranyl monophosphate (GP) [22,23], we hypothesized that enzymes within the NUDIX enzyme family might possess the capability to hydrolyze isoprene pyrophosphates in the human cell. To investigate this, we screened an extensive panel of human NUDIX enzymes for activity with the isoprene pyrophosphates IPPP and DMAPP and found NUDT15 (EC3.6.1.9) and NUDT18 (EC3.6.1.58) to efficiently catalyze their hydrolysis. Moreover, we identified additional isoprene PPs as substrates of NUDT15 and NUDT18 of which GPP was found to be hydrolyzed with the highest catalytic efficiency. We present the crystal structure of NUDT15 in complex with the hydrolysis product GP demonstrating the active site's efficient accommodation of the hydrophobic isoprenoid moiety. In summary, our findings unveil previously unknown hydrolysis activities of human NUDT18 and NUDT15 with endogenous isoprene pyrophosphate substrates, suggesting a novel role for these enzymes in isoprene PP metabolism.

## Results

### NUDT15 and NUDT18 are efficient catalysts of isoprene PP hydrolysis

To investigate whether any of the human NUDIX enzymes possess the capability to catalyze the hydrolysis of physiologically relevant isoprene PPs, we screened an extensive panel of 17 human NUDIX enzymes for activity with DMAPP and IPPP. Inorganic phosphate (Pi), formed upon NUDIX enzyme-catalyzed hydrolysis, was detected using a malachite green-based assay and measurement of absorbance at 630 nm. Out of the enzymes tested, NUDT15 and NUDT18 displayed notable activity with these isoprene PPs, as shown in Fig. 2A. Next, we tested the activities of NUDT15 and NUDT18 with additional isoprene-PPs and compared them with activities toward their previously described substrates, 8-oxo-dGDP for NUDT18 and dGTP for NUDT15. At a substrate concentration of 100  $\mu\text{M}$  both NUDT15 and NUDT18 demonstrated significant hydrolysis activity with IPPP, DMAPP, GPP, and FPP as illustrated in

Fig. 2B. Notably, only NUDT18 catalyzed the hydrolysis of mevalonate pyrophosphate (MPP). Furthermore, NUDT18 exhibited a considerably higher specific activity with GGPP compared to NUDT15. In addition, we assessed the activity of *Escherichia coli* MutT, a bacterial homolog to NUDT1 and NUDT15, with GPP. However, no activity was detected (Fig. 2C), suggesting that the observed activity with isoprene pyrophosphates within the NUDIX family has evolved in the eukaryotic domain of life.

### LC-MS analysis reveals hydrolysis takes place between phosphate groups

To further analyze the hydrolysis reactions of GPP and FPP, these isoprene PPs were incubated with NUDT15 and NUDT18, and samples from the reaction mixtures were collected after different incubation times and subjected to LC-MS analysis. The detected mass ( $m/z = 257 [M + \text{Na}^+]$ ) of the product peak was consistent with GP formation after GPP hydrolysis catalyzed by both NUDT18 (Fig. 3A) and NUDT15 (Fig. 4A), similar to the observations for AtNUDX1-catalyzed hydrolysis of GPP [23]. The time-dependent hydrolysis of GPP could be effectively monitored and was completed for NUDT15 and NUDT18 after 60 and 90 min, respectively (Figs 3C and 4C). The faster conversion of GPP in the case of NUDT15 is likely due to the twofold higher concentration of NUDT15 compared to NUDT18 used in the assay. LC-MS analysis of FPP hydrolysis revealed a distinct peak with  $m/z = 325 [M + \text{Na}^+]$ , consistent with FP being the product after NUDT18 and NUDT15 catalyzed FPP hydrolysis (Figs 3B and 4B). In comparison to the hydrolysis of GPP, the hydrolysis of FPP is notably slower, especially for NUDT15, where hydrolysis appears to plateau at 50% conversion (Figs 3D and 4D). This may potentially be due to product inhibition of the enzyme or be due to low solubility of the hydrophobic FP product. Additionally, in Fig. 3A, an extra small peak is visible just below 1.6 min elution time after NUDT18 catalyzed hydrolysis of GPP for 180 min. This peak may represent GOH that is formed by NUDT18 catalyzed hydrolysis of the produced GP.

### Detailed kinetic analysis of NUDT15 and NUDT18 activity with isoprene PPs

To further investigate the kinetics of NUDT18 and NUDT15 catalyzed hydrolysis of the identified isoprene PP substrates, we produced saturation curves by measuring initial enzyme activity rates at 22  $^{\circ}\text{C}$  at a

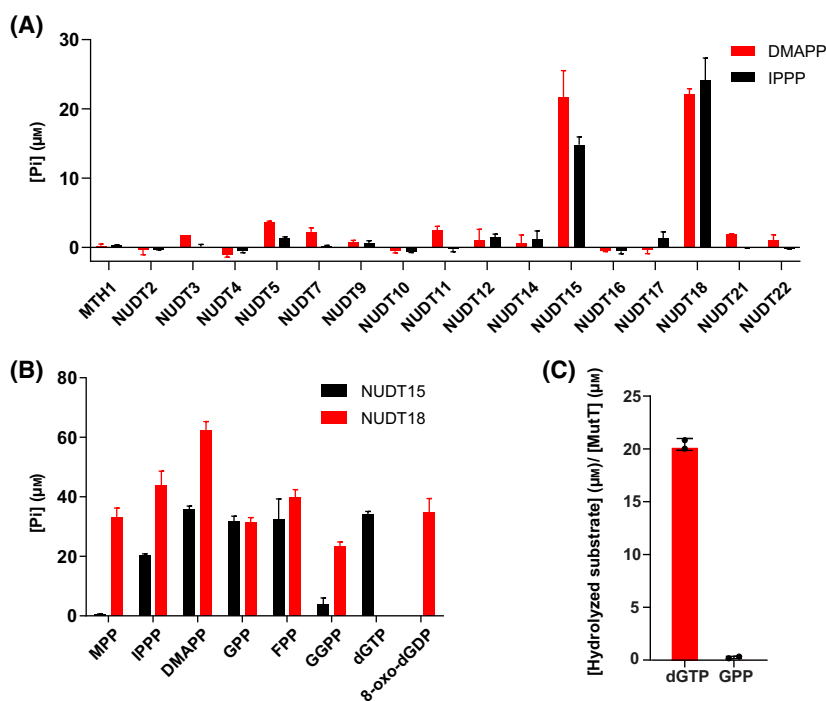


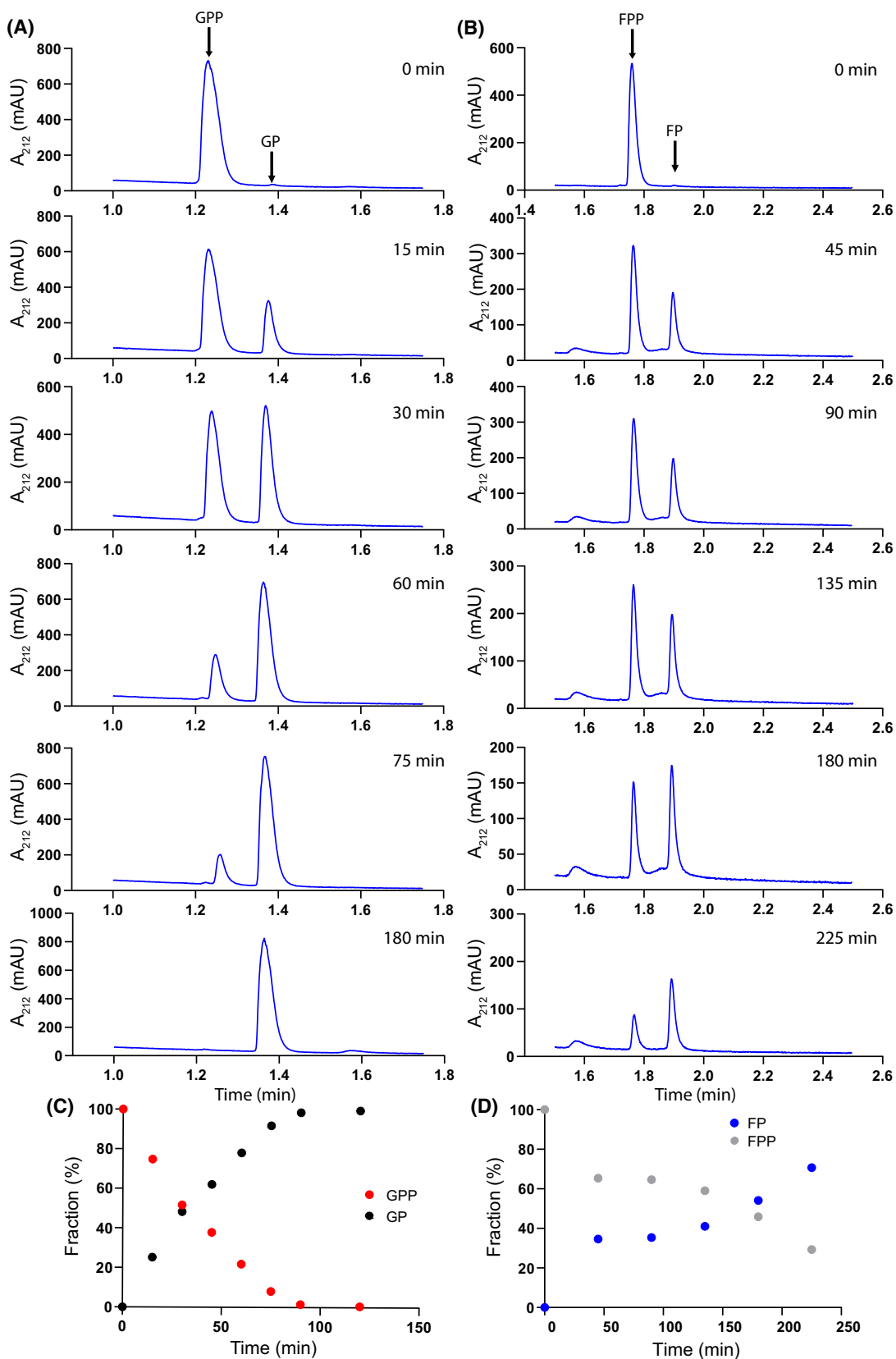
**Fig. 2.** NUDT15 and NUDT18 are catalysts of isoprene pyrophosphate hydrolysis. (A) A panel of 17 human NUDIX hydrolases was screened for activity with 100  $\mu\text{M}$  Dimethylallyl-PP (DMAPP) or isopentenyl-PP (IPPP) using 100 nM NUDIX enzyme. NUDT15 and NUDT18 were found to efficiently catalyze the hydrolysis of these isoprene PPs ( $n = 1$ ). (B) Activity of NUDT15 and NUDT18 (100 nM) was tested with isoprene PP substrates (100  $\mu\text{M}$ ) and compared with activity toward the previously known substrates dGTP for NUDT15 and 8-oxo-dGDP for NUDT18. Data are representative of two independent experiments ( $n = 2$ ). (C) *E. coli* MutT (50 nM), a bacterial homolog of MTH1 and NUDT15, was tested for activity with GPP (100  $\mu\text{M}$ ) and with dGTP (100  $\mu\text{M}$ ) as a positive control. No activity of MutT with GPP was detected. The graph shows data representative of two independent experiments with data points measured in duplicate. Error bars represent standard deviation.

range of substrate concentrations (Fig. 5A–C). The decision to assay the reaction rates at 22  $^{\circ}\text{C}$ , rather than the more physiologically relevant temperature of 37  $^{\circ}\text{C}$ , was based on the excessively rapid consumption of the substrates at 37  $^{\circ}\text{C}$ , which hindered accurate assessment of initial rates at the lower substrate concentrations. Determined kinetic parameters for NUDT18 and NUDT15 are presented in Tables 1 and 2, respectively. NUDT18 displays comparable turnover numbers for GPP, DMAPP, and IPPP, whereas the corresponding values for MPP and FPP are slightly lower. The  $K_m$ -value of NUDT18 was found to be lowest for GPP (3.7  $\mu\text{M}$ ) indicating that the affinity may be highest for this substrate, followed by

DMAPP, IPPP, FPP, GGPP, and MPP. The catalytic efficiency ( $k_{\text{cat}}/K_m$ ) of NUDT18 is highest for GPP followed by DMAPP, IPPP, FPP, MPP, and GGPP. However, the calculated low catalytic efficiency of NUDT18 with GGPP might be underestimated due to the limited solubility of this highly hydrophobic substrate (Fig. 1) in the aqueous assay buffer used. It is noteworthy that the catalytic efficiency of NUDT18 for the hydrolysis of GPP is considerably higher than that reported for its previously identified endogenous substrate, 8-oxo-dGDP [24].

GPP was also found to be the preferred substrate for NUDT15 among the isoprene pyrophosphates tested (Fig. 5C and Table 2). NUDT15 exhibits the

**Fig. 3.** LC–MS analysis of NUDT18 catalyzed hydrolysis of GPP and FPP reveals the formation of isoprene monophosphates. HPLC analysis showing that hydrolysis takes place between the phosphate groups in GPP and FPP and produces GP and FP. NUDT18 catalyzed hydrolysis of GPP (A) and FPP (B) was followed over time by incubation of GPP or FPP with NUDT18 and analysis of reaction mixture at different time points using HPLC and MS. The fraction of hydrolyzed substrate and formed product was calculated for GPP hydrolysis (C) and FPP hydrolysis (D) using the area under the curve of the peaks. Presented data are representative of two independent experiments.



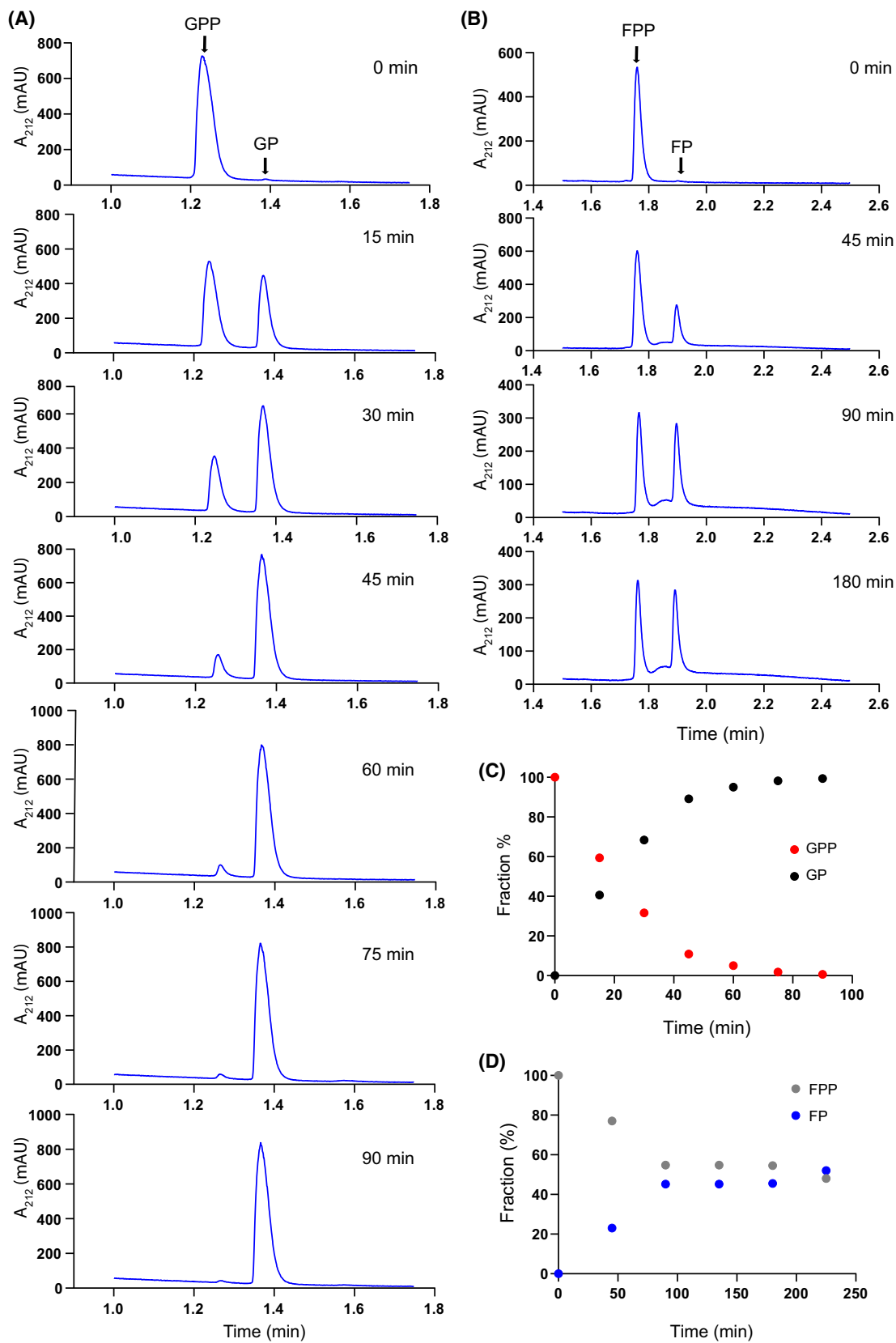


**Fig. 4.** LC–MS analysis of NUDT15 catalyzed hydrolysis of GPP and FPP reveals the production of isoprene monophosphates. HPLC analysis showing that hydrolysis takes place between the phosphate groups and produces GP and FP. NUDT15 catalyzed hydrolysis of GPP (A) and FPP (B) was followed over time by incubation with NUDT15 and sampling at different time points. Samples were analyzed using HPLC and MS and the fraction of hydrolyzed substrate and formed product was calculated for GPP hydrolysis (C) and FPP hydrolysis (D) using the area under the curve of the corresponding peaks. Data are representative of two independent experiments.

highest  $k_{\text{cat}}$ -value ( $0.7 \text{ s}^{-1}$ ) and the lowest  $K_{\text{m}}$ -value ( $18.7 \mu\text{M}$ ) with GPP, resulting in a catalytic efficiency of  $39\,900 \text{ M}^{-1}\cdot\text{s}^{-1}$ . However, this value is over fivefold lower compared to the catalytic efficiency of NUDT18 with GPP. IPPP ranks as the second-best substrate for NUDT15, followed by DMAPP, with catalytic efficiencies of  $8300$  and  $6500 \text{ M}^{-1}\cdot\text{s}^{-1}$ , respectively.

### Co-crystallization and structure determination of the NUDT15-GP complex

In order to understand the binding mode of the isoprene PPs we co-crystallized NUDT15 with GPP. Extensive efforts were also made to produce crystals of NUDT18 with GPP and other isoprene PPs but without success. We solved the structure of human NUDT15 in complex with GP to  $1.70 \text{ \AA}$  resolution (PDB: [7R0D](#)). Data processing and refinement statistics are presented in Table 3. The tertiary structure of NUDT15 is a homodimer, consistent with biochemical studies that show the protein is also dimeric in solution [25]. The NUDT15 protomer is comprised of two  $\alpha$ -helices, seven  $\beta$  strands, and three  $3_{10}$ -helices (Fig. 6A).

The individual monomers of NUDT15 are virtually identical as indicated by the low rmsd value of  $0.37 \text{ \AA}$  for the corresponding  $\text{C}\alpha$ -atoms. The conserved NUDIX family motif (GX<sub>5</sub>EX<sub>7</sub>REVXEEXGU), which contains the residues required for magnesium binding and substrate hydrolysis, is located on  $\alpha$ -helix 1 and  $\beta$ -strand 4. After structure refinement, it was evident that each monomer had electron density consistent with a single GP, indicating efficient hydrolysis of the GPP substrate by NUDT15 during co-crystallization (Fig. 6A). The GP product is nicely accommodated within the active site and is positioned by two hydrogen bonds between the alpha-phosphate and His49 (which is itself supported by a hydrogen bond with Tyr92), along with extensive hydrophobic interactions with Gly15, Val16, Gly17, Leu45, Pro46, Gly47, Gly48, and Thr94 (Fig. 6B). Each active site also contains a single magnesium ion exhibiting ideal octahedral coordination with the catalytic residues Glu63, Glu66 and four ordered water molecules, three of which are additionally supported by the residues

Glu67, Glu113, and Lys116 (Fig. 6C). Comparison of hNUDT15-GP with the structure of hNUDT15 in complex with 6-thio-GMP shows the structures superimpose well, with a low rmsd value of  $0.47 \text{ \AA}$ . 6-thio-GMP occupies a deeper position in the binding pocket compared to GP and is coordinated by more extensive hydrogen bonds, including the sidechain of His49, the main-chain nitrogen of Gly137 and the main-chain oxygen of Leu45. 6-thio-GMP is also supported by numerous hydrophobic interactions involving Pro46, Gly47, Gly48, Tyr90, Phe135, and Leu138. Importantly, the alpha-phosphates of both GP and 6-thio-GMP occupy a similar position, as do the magnesium ions in each structure (Fig. 6D).

### Comparison of hNUDT15-GP and hNUDT18 structures

In order to identify structural features that are important for the activity of NUDIX enzymes with isoprene PPs we superimposed the structures of hNUDT15-GP and the hNUDT18 NUDIX domain (PDB: [3GG6](#)). This showed that while the core structures overlay adequately, there are some regions that do not superimpose particularly well (rmsd for all C-alpha atoms of  $2.44 \text{ \AA}$ , amino acid sequence identity 29%) (Fig. 7A). This is in part due to small conformational changes that occur upon substrate binding, which are not observed in the ligand- and metal-free NUDT18 structure. Analysis of the ligand binding pocket shows there is sufficient space for isoprenoid substrates in the NUDT18 active site (Fig. 7B). Many of the hydrophobic interactions involved in GP binding and residues required for metal binding are conserved between the structures (Fig. 7B,C). However, there are also notable differences between hNUDT15 and hNUDT18. Interestingly, it is evident that the binding pocket of NUDT18 has a greater abundance of hydrophobic residues than the binding pocket of NUDT15 (Fig. 7B, C). In addition, differences in shape complementarity between NUDT15 and NUDT18 and the isoprene substrate might result in one of the proteins having more favorable van der Waals interactions with the substrate. This could be a contributing factor for the higher catalytic efficiency observed for NUDT18



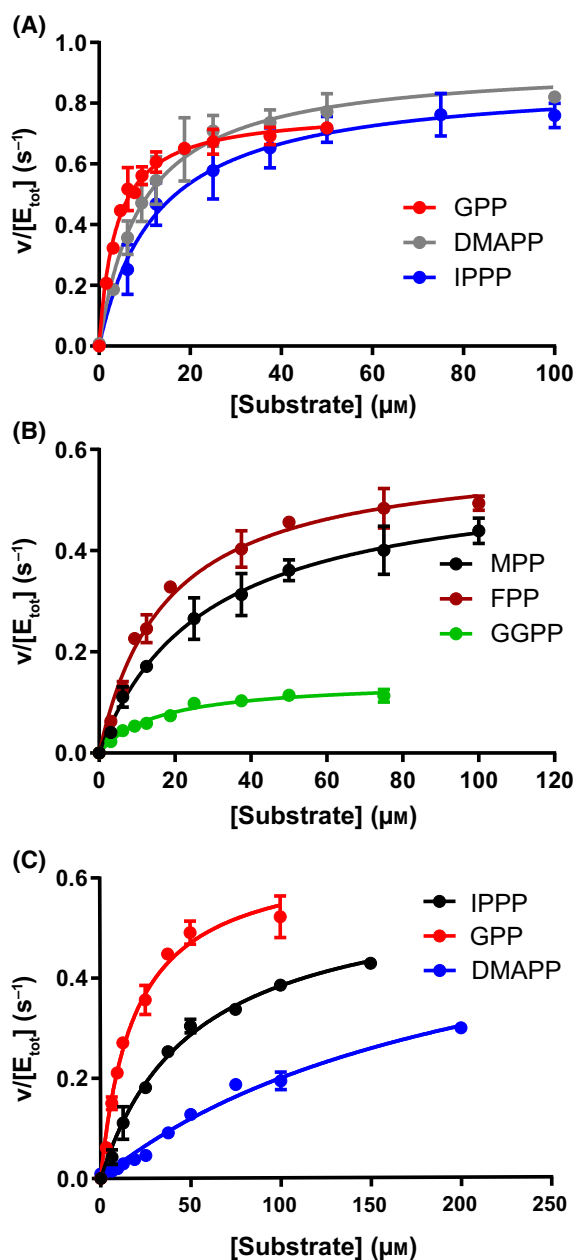


**Fig. 5.** NUDT18 and NUDT15 are efficient catalysts of GPP hydrolysis. (A) Saturation curves of NUDT18 with GPP, DMAPP, and IPPP. (B) Saturation curves of NUDT18 with MPP, FPP, and GGPP. (C) Saturation curves of NUDT15 with GPP, DMAPP, and IPPP. Graphs show saturation curves with data points representing average and standard deviation from two independent experiments ( $n = 2$ ), in which initial rates were determined using enzyme activities assayed in duplicate at three different time points.

toward GPP compared to NUDT15. Two other important differences include His49 and Thr92, which are both arginine residues (Arg77 and Arg117) in

NUDT18 (Fig. 7C). As shown in our hNUDT15-GP structure, His49 hydrogen bonds with the phosphate group of GP through nitrogen atoms in both its main chain and sidechain (Fig. 6B), suggesting that an arginine at this position should similarly fulfill this role. Arg117 in NUDT18 is particularly interesting in the context of substrate specificity toward MPP. Unlike the other isoprenoids we examined which have hydrophobic core structures, MPP contains a carboxyl group (Fig. 1) that would not be favored in the hydrophobic binding pocket. Based on our superpositions, only NUDT18 has a residue (Arg117) within hydrogen bonding range of MPP. This may be one reason why NUDT18 is capable of hydrolyzing MPP, whereas NUDT15 is unable to do so.

### Comparison of hNUDT15-GP and AtNUDT1-isopentyl-PP structures

NUDT1 from *Arabidopsis thaliana* has been reported to exhibit activity with isoprene PPs [23]. Comparison of the structures of hNUDT15-GP and AtNUDT1-Isopentyl-PP (PDB: 6DBZ) [26] reveals that the core structures superimpose quite well as indicated by the low rmsd value of 1.34 Å for their C-alpha atoms (amino acid sequence identity 42%) (Fig. 8A). Although a structure of AtNUDT1 in complex with GPP has been determined (PDB: 5GP0), it lacks magnesium ions necessary for proper substrate coordination [23]. We, therefore, focused our comparisons on the available AtNUDT1 Isopentyl diphosphate complex, where the substrate is coordinated by three magnesium ions [26]. Interestingly, when comparing ligand binding in AtNUDT1-Isopentyl-PP with our hNUDT15-GP structure, the hydrophobic portions of both Isopentyl-PP and GP occupy slightly different positions, as do their alpha-phosphates. In fact, the alpha-phosphate of GP superimposes more closely with the beta-phosphate of Isopentyl-PP (Fig. 8B), which may indicate that the hNUDT15-GP product complex itself might not represent a productive substrate binding mode. Residues involved in magnesium coordination are completely conserved between the structures, and the single magnesium in hNUDT15-GP occupies the same position as the second magnesium in the AtNUDT1-Isopentyl-PP structure (Fig. 8A,B). This positioning may provide the enzyme with the flexibility to accommodate molecules with different numbers of phosphate groups, enabling NUDT15 to efficiently hydrolyze both di- and triphosphate substrates. Upon comparing the GP-binding sites, we observed that Gly15 and Gly17 in hNUDT15 correspond to alanine and valine in AtNUDT1 (Fig. 8C).

**Table 1.** Kinetic parameters for NUDT18 with isoprene pyrophosphates. Values were calculated from kinetic parameters determined by fitting the Michaelis–Menten equation to initial rates determined at a range of substrate concentrations. *n*, number of independent experiments; SD, standard deviation.

Kinetic parameter	Substrate					
	MPP	IPPP	DMAPP	GPP	FPP	GGPP
<i>n</i>	2	2	2	2	2	2
$k_{\text{cat}}/K_m$ ( $\text{M}^{-1}\cdot\text{s}^{-1}$ )						
Mean	20 400	72 100	99 700	214 300	27 500	8500
SD	400	19 800	27 500	25 900	900	1200
$K_m$ ( $\mu\text{M}$ )						
Mean	26.8	12.4	9.8	3.7	18.8	17.9
SD	2.8	2.6	2.9	0.4	3.9	3.4
$k_{\text{cat}}$ ( $\text{s}^{-1}$ )						
Mean	0.55	0.87	0.94	0.78	0.52	0.15
SD	0.07	0.05	0.01	0.02	0.12	0.01

**Table 2.** Kinetic parameters for NUDT15 with isoprene pyrophosphates. The presented kinetic parameter values were determined by fitting the Michaelis–Menten equation to initial rates, determined at a range of substrate concentrations. *n*, number of independent experiments; SD, standard deviation.

Kinetic parameter	Substrate				
	GPP	IPPP	DMAPP	FPP	GGPP
<i>n</i>	2	2	2	1	1
$k_{\text{cat}}/K_m$ ( $\text{M}^{-1}\cdot\text{s}^{-1}$ )					
Mean	39 860	8330	6470	1350	870
SD	7160	4370	4770		
$K_m$ ( $\mu\text{M}$ )					
Mean	18.7	63.6	159.3	76.3	163.3
SD	0.2	19.4	40.5		
$k_{\text{cat}}$ ( $\text{s}^{-1}$ )					
Mean	0.72	0.49	0.94	0.10	0.10
SD	0.11	0.11	0.50		

In the AtNUDT1-Isopentyl-PP complex, the ligand forms hydrogen bonds with His42, Gly40, and Glu60, which are entirely conserved in hNUDT15. The substrate is also positioned by hydrophobic interactions involving Ala11, Tyr87, and Phe127. These residues are conserved with hNUDT15 except for Ala11 which is a glycine residue in the human enzyme (Fig. 8C). Notably, AtNUDT1, like NUDT18, has a more hydrophobic binding pocket compared to NUDT15, potentially explaining why these enzymes hydrolyze isoprene PPs much more efficiently than NUDT15 [26] as the binding of the hydrophobic portion of the isoprenoid substrates rely on hydrophobic interactions. Clearly, even small differences here can result in large differences in terms of binding affinity and catalytic efficiency toward the isoprene-PP substrates.

**Table 3.** Data collection and refinement statistics. Values in parentheses are for the highest-resolution shell.

NUDT15-GP	
PDB code	7R0D
Data collection	
Space group	P2 <sub>1</sub> 2 <sub>1</sub>
Cell dimensions	
<i>a</i> , <i>b</i> , <i>c</i> (Å)	46.7, 48.3, 135.2
$\alpha$ , $\beta$ , $\gamma$ (°)	90.0, 90.0, 90.0
Resolution (Å)	46.6–1.70 (1.73–1.70)
No. observations	388 242 (8976)
No. unique reflections	34 417 (1759)
<i>R</i> <sub>merge</sub>	0.07 (0.53)
CC (1/2)	0.99 (0.90)
<i>I</i> / $\sigma$ <i>I</i>	17.8 (2.6)
Completeness (%)	99.7 (96.7)
Redundancy	11.3 (5.1)
Refinement	
Resolution (Å)	45.5–1.70
No. reflections	32 621
<i>R</i> <sub>work</sub> / <i>R</i> <sub>free</sub> (%)	18.4/22.6
No. of atoms	
Protein	2974
Ligand	30
Metal	2
Water	172
<i>B</i> -factors	
Protein (Å <sup>2</sup> )	29.4
Ligand/ion (Å <sup>2</sup> )	52.3
Metal (Å <sup>2</sup> )	34.7
Water (Å <sup>2</sup> )	35.7
RMSDs	
Bond lengths (Å)	0.012
Bond angles (°)	1.71

### His49 is crucial for GPP hydrolysis activity

Based on our structural comparisons of hNUDT15-GP with existing NUDT15 and AtNUDT1 complexes,

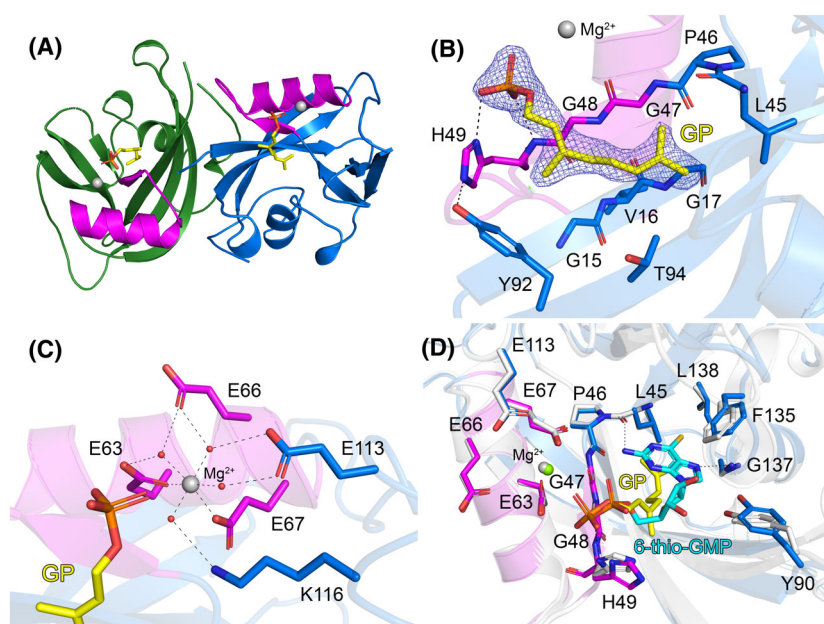


**Fig. 6.** Crystal structure of NUDT15 in complex with GP. (A) Overall structure of the NUDT15 dimer is depicted as a ribbon representation. Each monomer is colored green and blue, respectively. The highly conserved NUDIX motif is colored magenta. The product GP is shown as a stick representation with its respective atoms colored; carbons yellow, oxygens red, and phosphorus atoms orange. The magnesium ions required for activity and ligand coordination are shown as gray spheres. (B) Active site hydrogen bond network of GP. Residues contributing to ligand binding are labeled by residue number. Nitrogen and oxygen atoms are colored blue and red, respectively. Hydrogen bond interactions are shown as dashed lines. The calculated  $2F_o - F_c$  electron density map around GP is shown in blue, contoured at  $1.0 \sigma$  and the  $F_o - F_c$  electron density maps are green and red contoured at  $+3.5 \sigma$  and  $-3.5 \sigma$ , respectively. (C) Hydrogen bond network showing magnesium coordination in the active site. Water molecules are shown as red spheres. (D)  $\text{C}\alpha$ -atom superposition of hNUDT15-GP (coloring identical to panels A–C) with hNUDT15-6-thio-GMP (colored white; PDB ID: 5LPG). The hydrogen bond network for 6-thio-GMP is shown and the bound magnesium ion is shown as a green sphere. 6-thio-GMP is shown as a stick model with its atoms colored; carbons cyan, nitrogens blue, oxygens red, phosphorus atoms orange, and sulfurs gold. Figures were produced with PYMOL (v.2.3.3, Schrödinger, LLC, New York, NY, USA).

it is evident that residue His49 plays a crucial role in positioning the phosphate group of the substrate, as well as stabilizing the monophosphate product. To investigate the impact of this residue on catalytic activity, we generated the NUDT15H49A mutant and determined the activities of NUDT15wt and NUDT15H49A with dGTP and GPP (Fig. 9A). At presumably saturating concentrations of the two substrates ( $100 \mu\text{M}$ ) the H49A mutation causes a dramatic decrease in activity for both substrates. To investigate the role of the H49A mutation in more detail we produced saturation curves for NUDT15wt and NUDT15H49A with GPP (Fig. 9B) and dGTP (Fig. 9C) and determined kinetic parameters (Table 4). The H49A mutation led to a 30-fold reduction of the  $k_{\text{cat}}$ -value for GPP while causing only a twofold drop in the  $k_{\text{cat}}$ -value for dGTP. However, the introduction of the H49A mutation resulted in a 14-fold increase in the  $K_m$ -value for dGTP leading to a 28-fold reduction in catalytic efficiency. Determining an exact  $K_m$ -value for GPP is not possible due to the very low activity of NUDT15H49A with this substrate. It appears that the

His49A mutation has a more pronounced negative impact on the  $k_{\text{cat}}$ -value of NUDT15 catalyzed hydrolysis of GPP compared to dGTP, which may in part be due to the hydrogen bond made by this histidine having better geometry with GPP, which would make it stronger. Overall, it is evident that the H49A mutation affects the catalytic activity of NUDT15 with both GPP and dGTP. The saturation kinetics experiments for NUDT15wt and NUDT15H49A were conducted using assay buffer without the detergent Tween 20. The rationale behind this was to align with assay conditions previously used for assaying activity with dGTP. In the absence of the detergent the activity of NUDT15wt with GPP was lower compared to the activity with dGTP (as shown in Fig. 9B,C), contrary to the specific activity of NUDT15wt with GPP and dGTP (Fig. 9A) determined in assay buffer containing Tween 20. The absence of the detergent in the assay buffer likely accounts for the lower  $k_{\text{cat}}$  and  $k_{\text{cat}}/K_m$  values of NUDT15wt toward GPP (4.8- and 8.6-fold, respectively), as presented in Table 4, compared to the values presented for NUDT15wt in Table 2. These

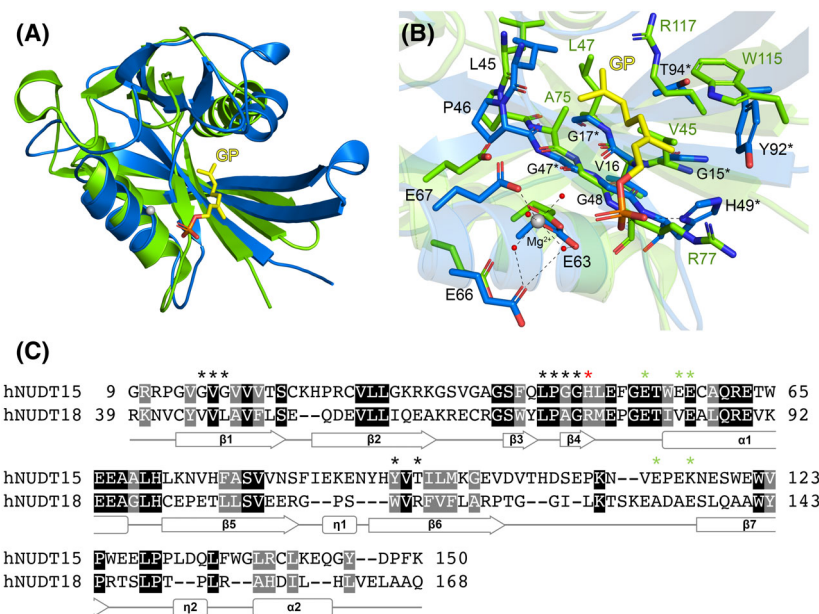


**Fig. 7.** Structural comparison of hNUDT15-GP with the hNUDT18 nucleotidase domain. (A) Superposition of hNUDT15-GP (blue) and hNUDT18 (green, PDB ID: 3GG6) monomers. GP is shown as a yellow stick model with the coordinated magnesium ion shown as a gray sphere. (B) Comparison of the residues involved in the coordination of GP and magnesium in the hNUDT15-GP structure. Residue numbering represents the hNUDT15 structure and in cases where the residue is not conserved, the residue from hNUDT15 is labeled with an asterisk, and the corresponding residue from hNUDT18 is labeled in dark green. Nitrogen, oxygen, and phosphorus atoms are colored blue, red, and orange, respectively. Water molecules are shown as small blue spheres. Hydrogen bond interactions are shown as dashed lines. (C) Amino acid sequence alignment of human NUDT15 (UniProt: Q9CA40) and the nucleotidase domain of human NUDT18 (Q6ZVK8) were performed using CLUSTAL OMEGA (EMBL-EBI, Hinxton, UK) through the EBI webserver. The resulting alignment is colored according to sequence similarity using BOXSHADE (written by Kay Hofmann and Michael Baron, Swiss Institute of Bioinformatics, Switzerland). Identical residues are shaded black, while gray shading indicates amino acids with conserved physicochemical properties. Residues in hNUDT15 which form hydrogen bond or hydrophobic interactions with GP are shown as asterisks, colored red and black, respectively. Green asterisks indicate residues required for magnesium coordination. The secondary structure corresponding to the amino acid sequence of hNUDT15-GP is displayed below the alignment.

discrepancies can likely be attributed to an increased solubility of GPP in the presence of 0.01% Tween 20, resulting in more substrate available for hydrolysis.

### Analysis of NUDT15 and NUDT18 expression in noncancerous and cancerous cells

Small GTPases require prenylation for their localization to cellular membranes, where they exert their specific functions. Certain GTPases are instrumental in processes such as cell proliferation, cell survival, and cell signaling [5]. Variations in the cellular concentrations of NUDT15 and NUDT18 may lead to different levels of isoprenylation due to the modulation of concentrations of metabolites necessary for producing the isoprenylation substrates, FPP and GGPP. Consequently, variations in the expression levels of *NUDT15* and *NUDT18* could potentially impact cell proliferation. In order to investigate whether any differences in expression levels of the *NUDT15* and *NUDT18* genes can be observed in noncancerous compared to

cancerous cells, we analyzed RNA-seq data from a large panel of cell lines and sorted these cell lines based on noncancerous, cancerous, and tissue origin. Interestingly, the expression of *NUDT18* was found to be significantly higher in noncancerous compared to cancerous cell lines (Fig. 10A). The largest difference in *NUDT18* expression level was observed between noncancerous cell lines and cell lines originating from cervical cancer and neuroblastoma with 33- and 37-fold difference in expression level, respectively (Table 5). However, no such difference in expression level between carcinogenic and noncarcinogenic cell lines was observed for *NUDT15* (Fig. 10B).

## Discussion

### A novel activity of NUDT15 and NUDT18 in catalysis of isoprene PP hydrolysis

NUDT18 was initially identified as an enzyme capable of catalyzing the hydrolysis of 8-oxo-dGDP to

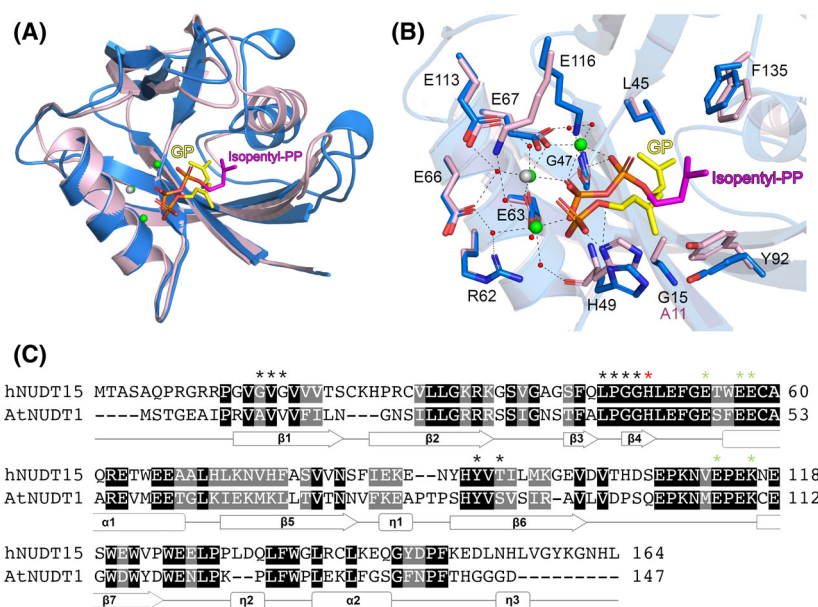


**Fig. 8.** Structural comparison of hNUDT15-GP with AtNUDT1-Isopentyl-PP. (A) Superposition of hNUDT15-GP (blue) and AtNUDT1 (light pink, PDB ID: 6DBZ) monomers. GP and Isopentyl-PP are shown as sticks, colored yellow and magenta, respectively. Magnesium ions are colored gray (hNUDT15) or green (AtNUDT1). (B) Comparison of the residues involved in the coordination of isopentyl-PP and magnesium in the AtNUDT1-Isopentyl-PP structure. Residue numbering represents the hNUDT15 structure and in cases where the residue is not conserved, the relevant residue from AtNUDT1 is labeled in dark pink. Nitrogen, oxygen, and phosphorus atoms are colored blue, red, and orange, respectively. Water molecules are shown as red spheres. Hydrogen bond interactions are shown as dashed lines. (C) Amino acid sequence alignment of human NUDT15 (UniProt: Q9CA40) and *A. thaliana* NUDT1 (Q9NV35) was performed using CLUSTAL OMEGA through the EBI webserver. The resulting alignment is colored according to sequence similarity using BOXSHADE. Identical residues are shaded black, while gray shading indicates amino acids with conserved physicochemical properties. Residues in hNUDT15 which form hydrogen bond or hydrophobic interactions with GP are shown as asterisks, colored red and black, respectively. Green asterisks indicate residues required for magnesium coordination. The secondary structure corresponding to the amino acid sequence of hNUDT15-GP is displayed below the alignment. Figures were produced with PYMOL (v.2.3.3, Schrödinger).

8-oxo-dGMP, suggesting a role in protecting against mutagenesis and DNA damage resulting from the incorporation of 8-oxo-dG into DNA [27]. However, subsequent findings revealed that the depletion of NUDT18 neither increased the sensitivity to hydrogen peroxide nor did the overproduction of NUDT18 in MutT-deficient *E. coli* suppress the mutator phenotype [28]. This implies that NUDT18 may not primarily function in safeguarding the genome against oxidative stress but likely serves other cellular roles. NUDT15, closely related to NUDT1 (MutT homolog 1, MTH1) and commonly referred to as MTH2, was initially thought to act as a redundancy factor for MTH1 by catalyzing the hydrolysis of the mutagenic 8-oxo-dGTP [29]. However, NUDT15 was found to exhibit a very weak 8-oxo-dGTP activity compared to MTH1, and no increase in 8-oxo-dG in DNA was observed upon NUDT15 depletion, questioning this view [25]. Recent studies have revealed significant roles for NUDT15 in the metabolism of anti-cancer drugs (thiopurines) and antiviral drugs (aciclovir and ganciclovir)

[30–33]. However, the natural functions of NUDT15 have remained elusive.

Here, we present data showing that NUDT15 and NUDT18 exhibit pronounced activities with physiologically relevant isoprene PPs, suggesting a potential previously completely unknown novel cellular function for these enzymes. In comparison to previously reported activities of NUDT15 and NUDT18 with endogenous substrates, both enzymes demonstrate considerably higher catalytic efficiencies toward GPP. For NUDT18, the catalytic efficiency with GPP is approximately twice as high as the reported catalytic efficiency with 8-oxo-dGDP [24]. Similarly, for NUDT15, the catalytic efficiency for GPP hydrolysis exceeds by 10-fold the reported value for this enzyme with 8-oxo-dGTP [25].

### Evolutionary conservation of isoprene PP hydrolysis in vertebrates

In order to identify residues in NUDT15 that have been conserved during evolution, we conducted a

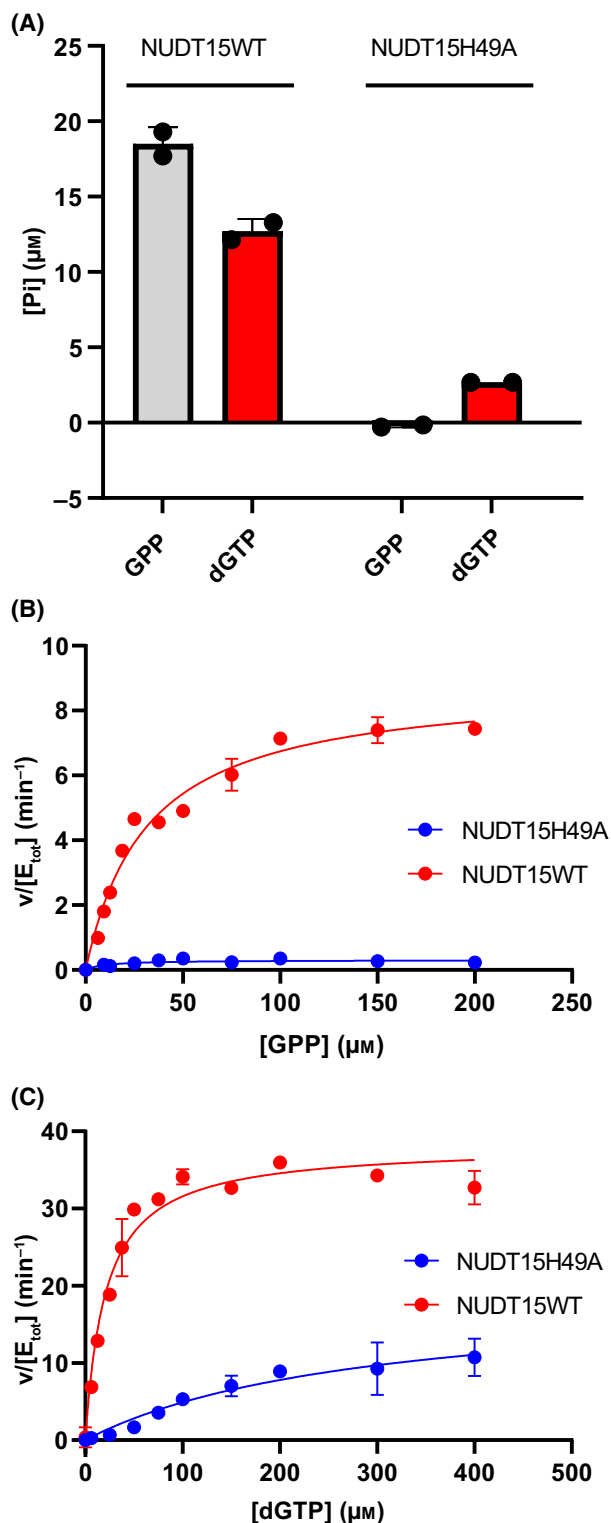


**Fig. 9.** Mutation of His49 drastically decreases hydrolysis activity with dGTP and GPP. (A) Activity was tested using 100 µM dGTP (red bars) or GPP (gray bars) and 100 nM NUDT15WT or NUDT15H49A at 22 °C. Data are presented as mean and standard deviation (SD) and are representative of two experiments ( $n = 2$ ). (B) Saturation curves of NUDT15WT and NUDT15H49A were produced by determining initial rates using 50 nM NUDT15 WT and 100 nM NUDT15H49A and substrate concentrations of GPP ranging from 0 to 200 µM. (C) Saturation curves with dGTP were produced by determining initial rates of 5 nM NUDT15WT or 50 nM NUDT15H49A at dGTP concentrations between 0 and 400 µM. Graphs show saturation curves with data points representing mean and SD from two independent experiments ( $n = 2$ ) in which initial rates were determined using enzyme activities assayed in duplicate at three different time points.

His49, the only active site residue forming a hydrogen bond in the hNUDT15-GP structure, is entirely conserved. Residues that coordinate magnesium are also completely conserved across the sequences with a single exception of Glu66, which is a glutamate in all sequences except for chicken NUDT15. The residues involved in hydrophobic interactions in the NUDT15-GP complex are generally conserved, except for Gly15, Val16, and Gly17, which are replaced by larger hydrophobic residues in some of the other sequences. This observation aligns well with what we observed in the hNUDT18 and AtNUDT1 structures, suggesting that other vertebrate NUDT15 enzymes should also be capable of hydrolyzing isoprene PPs. In addition, we performed a multiple sequence alignment of NUDT18 proteins from humans and a range of other vertebrates (Fig. 12). All residues predicted to interact with the isoprenoids are fully conserved, indicating that NUDT18 enzymes from other vertebrate species would likely exhibit activity with isoprene PPs as well.

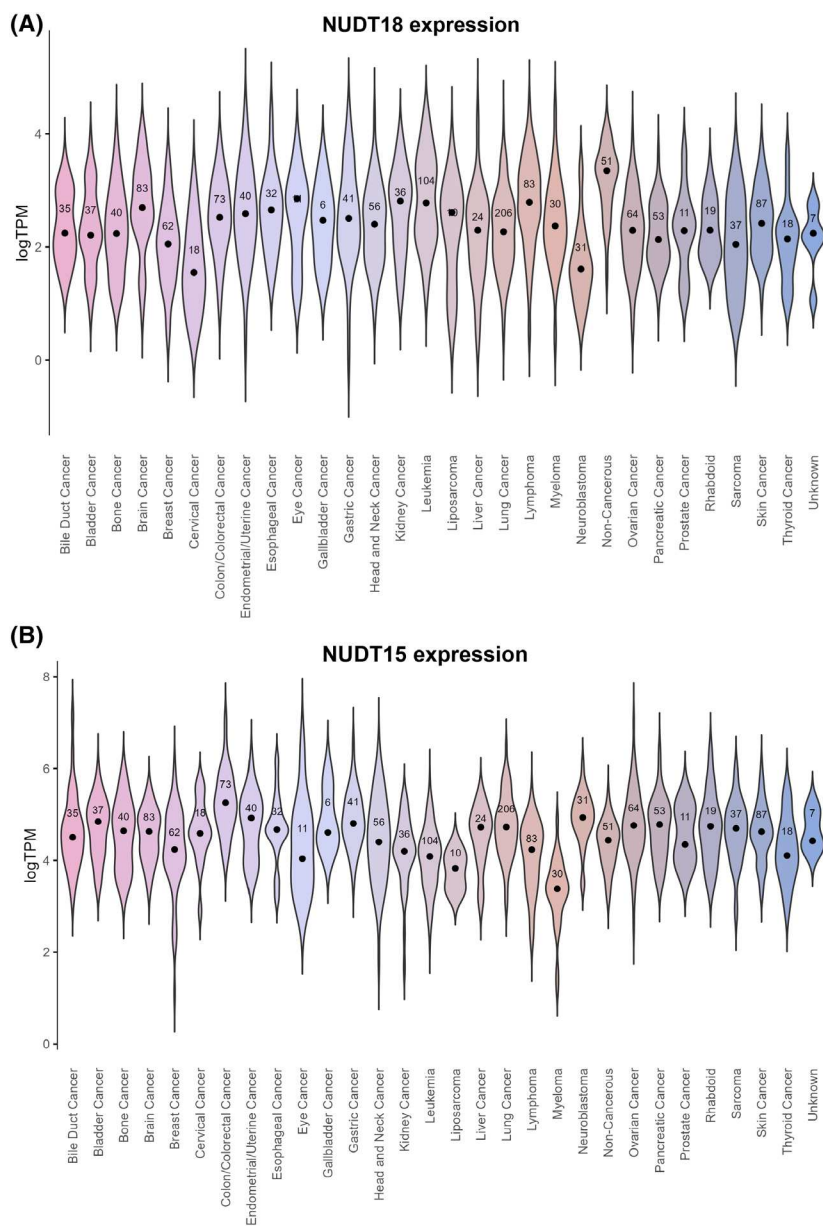
### Relevance of NUDIX enzyme catalyzed isoprene PP hydrolysis in the cell

Figure 13 illustrates the isoprene biosynthesis pathway leading to the production of cholesterol and other biomolecules and highlights the enzymes that are involved in isoprene PP metabolism in animals. The activities of NUDT18 and NUDT15 with isoprene PPs that we report here suggest that these enzymes may have a role in modulating the cellular levels of these metabolites and, consequently their downstream products. Hydrolysis of GGPP and FPP, or other isoprene PPs used for their production, would decrease the concentration of available substrates for geranylgeranylation and farnesylation, respectively. This reduction could lead to a decrease in the localization of small GTPases to

multiple sequence alignment involving the human NUDT15 protein and a curated array of NUDT15 proteins from various vertebrate species (Fig. 11).

**Table 4.** Kinetic parameters for NUDT15WT and NUDT15H49A with GPP and dGTP. The presented kinetic parameter values were determined by fitting the Michaelis Menten equation to initial rates determined at a range of substrate concentrations. Data are representative of two independent experiments ( $n = 2$ ). nd, not determined; SD, standard deviation.

	GPP			dGTP		
	$k_{cat}$ ( $\text{min}^{-1}$ )	$K_M$ ( $\mu\text{M}$ )	$k_{cat}/K_M$ ( $\text{M}^{-1}\cdot\text{min}^{-1}$ )	$k_{cat}$ ( $\text{min}^{-1}$ )	$K_M$ ( $\mu\text{M}$ )	$k_{cat}/K_M$ ( $\text{M}^{-1}\cdot\text{min}^{-1}$ )
NUDT15WT						
Mean	9.05	32.4	279 660	34.9	22.3	1 577 250
SD	0.21	0.9		4.7	1.8	
NUDT15H49A						
Mean	0.32	nd	nd	22.0	378	59 650
SD	0.02			4.2	126	



**Fig. 10.** Expression analysis of *NUDT18* (A) and *NUDT15* (B) in noncancerous and cancerous cell lines grouped based on tissue origin showing higher expression of *NUDT18* in noncancerous cell lines. Analysis of variance (ANOVA) was applied to RNA-seq data from 1408 cell lines to identify differences in gene expression between cell lines originating from different tissues and grouped as noncancerous or cancerous. The number of cell lines in each group is indicated. ANOVA  $P$  value was  $2.75 \times 10^{-33}$  for *NUDT18* and  $6.50 \times 10^{-50}$  for *NUDT15*. TPM, Transcripts per million. Figure was prepared using the software R version 4.1.3 (R Core Team, Vienna, Austria).

**Table 5.** Tukey *post hoc* test of *NUDT18* expression in noncarcinogenic and carcinogenic cell lines. CI, 95% confidence interval. Listed are pairs displaying an adjusted *P* value below 0.0001.

Pairs compared	Difference (means, log TPM)	Lower CI	Upper CI	<i>P</i> value (adjusted)
Noncancerous-neuroblastoma	1.5276	0.8979	2.1574	1.2529E-12
Noncancerous-breast cancer	1.1540	0.6313	1.6767	1.3146E-12
Noncancerous-lung cancer	0.9201	0.4876	1.3526	1.9839E-12
Neuroblastoma-leukemia	-1.1751	-1.7409	-0.6093	4.3029E-12
Noncancerous-cervical cancer	1.5737	0.8156	2.3317	4.3449E-12
Neuroblastoma-lymphoma	-1.1196	-1.7016	-0.5376	2.2776E-10
Sarcoma-noncancerous	-1.1409	-1.7380	-0.5438	3.2419E-10
Pancreatic cancer-Noncancerous	-0.9807	-1.5231	-0.4384	4.8485E-09
Ovarian cancer-Noncancerous	-0.9375	-1.4565	-0.4185	5.0824E-09
Leukemia-breast cancer	0.8014	0.3578	1.2451	5.0848E-09
Neuroblastoma-brain cancer	-1.0433	-1.6253	-0.4613	7.2509E-09
Leukemia-cervical cancer	1.2211	0.5152	1.9270	3.5095E-08
Lung cancer-leukemia	-0.5675	-0.9001	-0.2349	6.2752E-08
Lymphoma-cervical cancer	1.1656	0.4467	1.8846	4.7753E-07
Lymphoma-breast cancer	0.7459	0.2818	1.2101	6.6429E-07
Noncancerous-bone cancer	0.9151	0.3311	1.4991	1.6650E-06
Skin cancer-noncancerous	-0.7519	-1.2395	-0.2642	2.9217E-06
Cervical cancer-brain cancer	-1.0893	-1.8082	-0.3704	5.2592E-06
Noncancerous-head and neck cancer	0.8062	0.2710	1.3414	6.3742E-06
Sarcoma-leukemia	-0.7883	-1.3176	-0.2590	9.2157E-06
Thyroid cancer-Noncancerous	-1.1147	-1.8728	-0.3567	1.3772E-05
Noncancerous-bladder cancer	0.8713	0.2742	1.4684	1.7511E-05
Noncancerous-liver cancer	0.9920	0.3076	1.6764	2.1543E-05
Breast cancer-brain cancer	-0.6696	-1.1338	-0.2055	2.4720E-05
Neuroblastoma-colon/colorectal cancer	-0.8543	-1.44707	-0.2615	2.5499E-05
Neuroblastoma-kidney cancer	-0.9762	-1.6537	-0.2987	2.5667E-05
Lymphoma-lung cancer	0.5121	0.1526	0.8715	3.6070E-05
Noncancerous-bile duct cancer	0.8456	0.2387	1.4525	6.8016E-05
Neuroblastoma-endometrial/uterine cancer	-0.9096	-1.5712	-0.2479	9.8449E-05

cellular membranes, potentially affecting many cellular processes.

The question is whether the hydrolysis activity of NUDT15 and NUDT18 with isoprene PPs that we observe in our biochemical activity assay *in vitro* also takes place in a cellular context. We determined the catalytic efficiency of NUDT18 with GPP to  $2.1 \times 10^5 \text{ M}^{-1} \cdot \text{s}^{-1}$  at 22 °C, a value comparable to the reported catalytic efficiencies determined at 37 °C for geranylgeranyl pyrophosphate synthase (GGPPS) and Farnesyl pyrophosphate synthase (FPPS) [34,35], enzymes catalyzing the formation of GGPP and FPP in the cholesterol synthesis pathway, respectively (Fig. 13). The catalytic efficiency of NUDT18 at 37 °C is expected to be considerably higher than the catalytic efficiency determined at 22 °C, and consequently higher than the corresponding value for FPPS, which also uses GPP as substrate. This suggests that NUDT18 hydrolyzes GPP within the cell. Furthermore, the median  $k_{\text{cat}}/K_{\text{m}}$  value from a dataset comprising published values for approximately 1900

enzymes with their natural substrates is around  $1 \times 10^5$  [36]. The twofold higher catalytic efficiency of NUDT18 with GPP reported here supports the likelihood that GPP indeed is an endogenous substrate of NUDT18. Additionally, the low  $K_{\text{m}}$  value of NUDT18 for GPP (3.7  $\mu\text{M}$ ) (Table 1) is comparable to the  $K_{\text{m}}$  value of GGPPS for IPP and FPP [34,35], as well as the  $K_{\text{m}}$  values of FPPS for IPP and GPP [35]. This further backs up the hypothesis that NUDT18-catalyzed hydrolysis of GPP occurs within the cell.

GGOH and GOH are known key players in the feedback regulation of cholesterol production [12,37,38]. These isoprenoid alcohols have also been shown to act as cellular signaling molecules and to possess anti-inflammatory properties [39,40]. Additionally, the isoprenoid alcohol Farnesol (FOH) has been identified as an activator of the nuclear farnesoid X hormone receptor [41]. These findings suggest that isoprene alcohols play roles beyond regulating isoprene biosynthesis. The source of GGOH, GOH, and FOH are their corresponding isoprene pyrophosphates and



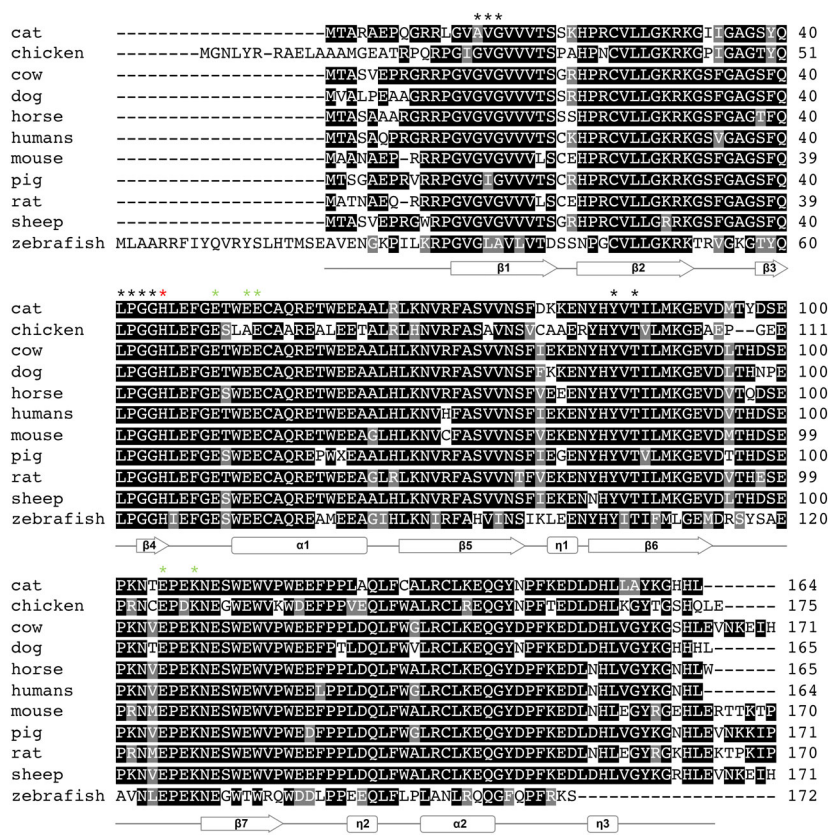


**Fig. 11.** Sequence alignment of NUDT15 proteins from humans and other species. NUDT15 amino acid sequences from *F. catus* (UniProt: A0A212U059), *G. gallus* (UniProt: F1NV92), *B. taurus* (UniProt: E1B7T3), *C. lupus* (UniProt: ER2DP5), *E. caballus* (UniProt: F7BQG1), *H. sapiens* (UniProt: Q9NV35), *M. musculus* (UniProt: Q8BG93), *S. scrofa* (UniProt: I3LBG2), *R. norvegicus* (UniProt: D3ZKQ0), *O. aries* (UniProt: A0A6P3TH16), and *D. rerio* (UniProt: Q6IQB3) were compared using CLUSTAL OMEGA through the EBI webserver. The resulting alignment is colored according to sequence similarity using BOXSHADE. Identical residues are shaded black, while gray shading indicates amino acids with conserved physicochemical properties. Residues from the hNUDT15-GP structure shown to form hydrogen bonds or hydrophobic interactions with GP are shown as asterisks, colored red and black, respectively. Green asterisks indicate residues required for magnesium coordination. The secondary structure corresponding to the amino acid sequence of hNUDT15-GP is displayed below the alignment.

enzyme-catalyzed hydrolysis is likely required for their production. How these isoprenoid alcohols are produced in human cells is not fully understood, however, the polyisoprenoid diphosphate phosphatase (PDP1), integrated into the ER membrane, has been demonstrated to hydrolyze GGPP, FPP, and GPP [18]. However, due to the membrane-bound nature of this enzyme and the use of micelles in activity experiments, a proper comparison of its activity with that of NUDT15 and NUDT18 with these isoprene PPs is not feasible. In contrast to PDP1, NUDT15, and NUDT18 are located in the soluble cytosolic fraction, like many other enzymes in the isoprenoid biosynthesis pathway such as GPPS and FPPS (Fig. 13) [42,43]. Our results suggest that NUDT15 and NUDT18 may be responsible for the hydrolysis of isoprene PPs in the cytosol. Alternatively, these NUDIX enzymes may act in concert with PDP1 in the production of isoprenoid alcohols. An isoprenoid shunt, capable of converting isoprenoid alcohols into isoprene PPs via phosphorylation of isoprenoid alcohols and monophosphates, and vice versa, has been postulated to exist (Fig. 13) [44]. The observed activities of NUDT15 and NUDT18 presented here imply a potential involvement of these enzymes in such a shunt.

We anticipate that our findings will inspire investigations into isoprene-dependent metabolites in clinical samples from patients carrying NUDT15 gene variants that result in low NUDT15 enzyme levels and consequently reduced cellular NUDT15 activity [32,45,46].

Cellular hydrolysis of the isoprene PPs, which constitute metabolites in the cholesterol synthesis pathway, could ultimately impact cholesterol production since FPP, which is utilized for the synthesis of cholesterol, is synthesized from GPP and DMAPP (Fig. 13). Elevated cellular levels of NUDT15 and NUDT18 may reduce cholesterol production by decreasing the concentration of intermediates in the cholesterol synthesis pathway. Both NUDT15 and NUDT18 exhibit low tissue specificity, being expressed in most tissues (Human Protein Atlas, <https://www.proteinatlas.org>), but interestingly, in the liver, where cholesterol production is high, the level of NUDT18 mRNA is very low and the protein is undetectable (Human Protein Atlas, <https://www.proteinatlas.org>).

When analyzing the expression of NUDT18 in a large panel of cell lines we observed a markedly elevated expression in noncancerous cell lines in comparison to cancerous counterparts (Fig. 10A and Table 5) indicating that downregulation of NUDT18 expression may

**Fig. 12.** Sequence alignment of the NUDT18 nucleotidase domain from humans and other species. NUDT18 nucleotidase amino acid sequences from *F. catus* (NCBI: XP\_003984764.1), *P. troglodytes* (UniProt: H2QVU3), *B. taurus* (UniProt: F1N0N5), *C. lupus* (UniProt: F1PDW5), *E. caballus* (UniProt: F6RHM5), *H. sapiens* (UniProt: Q6ZVK8), *M. musculus* (UniProt: Q3U2V3), *S. scrofa* (UniProt: F1RMB9), *R. norvegicus* (UniProt: Q641Y7), *O. aries* (UniProt: W5PLD7), and *D. rerio* (UniProt: Q568Q0) were compared using CLUSTAL OMEGA through the EBI webserver. The resulting alignment is colored according to sequence similarity using BOXSHADE. Identical residues are shaded black, while gray shading indicates amino acids with conserved physicochemical properties. Residues from human NUDT18 predicted to interact with isoprenoids (specifically GP) are shown as asterisks, colored red and black, respectively. Green asterisks indicate residues required for magnesium coordination. The secondary structure corresponding to the amino acid sequence of the hNUDT18 nucleotidase domain (PDB ID: 3GG6) is displayed below the alignment.

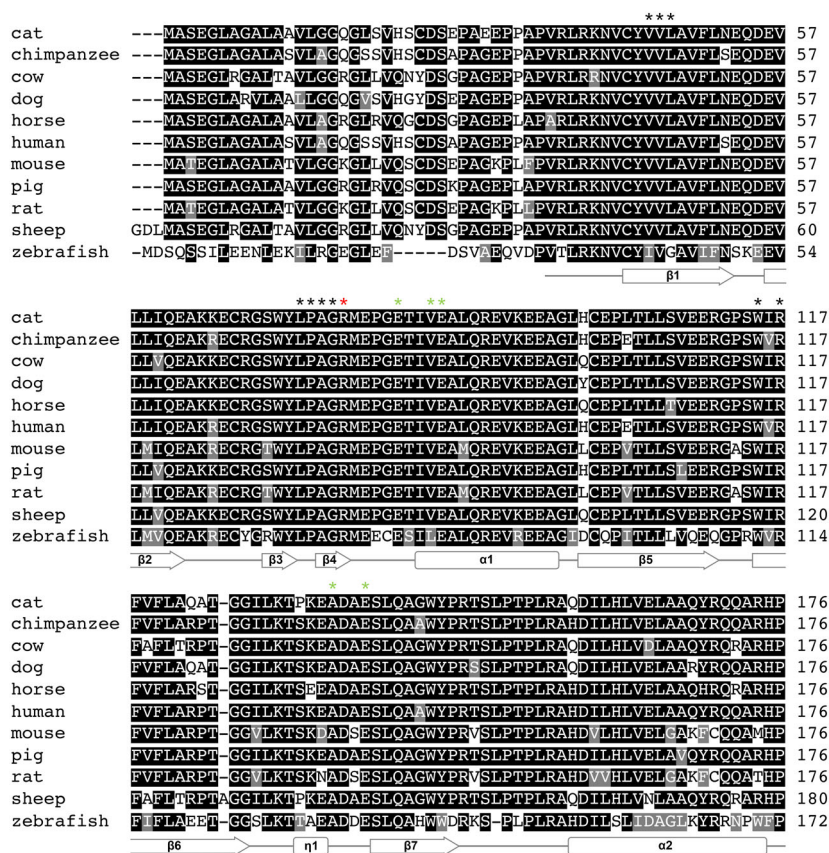
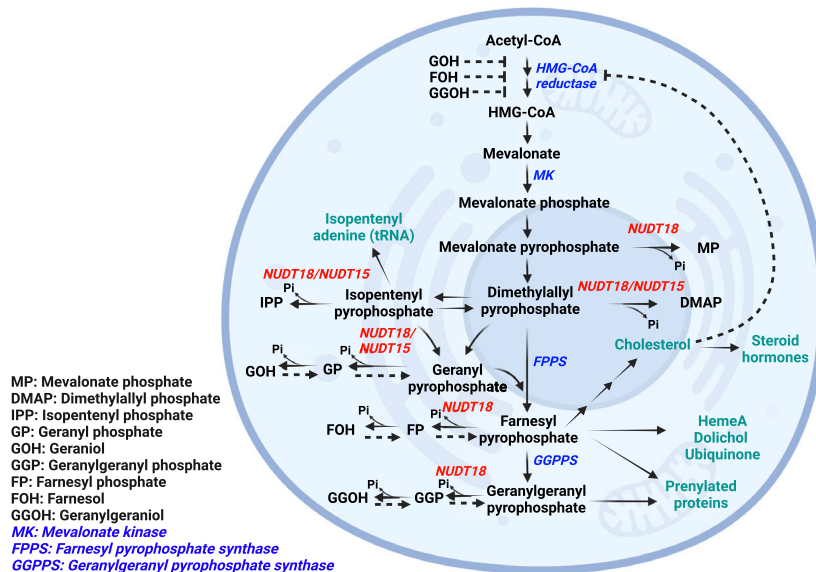


**Fig. 13.** Schematic figure of the biosynthetic pathways involving isoprene pyrophosphates in the human cell. The figure shows the biosynthetic pathways leading to cholesterol and other biomolecules (shown in dark cyan) in which the isoprene PPs discovered to be substrates for NUDT18 and NUDT15 are central. Enzymes discussed in the text are indicated in blue italics. NUDT15 and NUDT18 are indicated in red italics. Inhibition of HMG-CoA reductase by metabolites is indicated by dashed lines. Phosphorylation reactions are indicated by dashed arrows. The figure was created with Biorender.com.



occur during cell transformation. Such difference in expression levels between noncancerous and cancerous cell lines was not observed for NUDT15 (Fig. 10B), in line with NUDT15 displaying lower activity with

isoprene PPs compared to NUDT18. Interestingly, NUDT18 deficient cells have been reported to exhibit a noticeably reduced proliferation rate, implying a role of NUDT18 in cell growth [28]. We speculate that these

findings may be due to the involvement of NUDT18 in isoprene PP hydrolysis, which would modulate the availability of substrates for protein isoprenylation or other isoprene metabolites ultimately leading to alterations in proliferation. However, further investigations are needed to understand the specific impact of NUDT15 and NUDT18 activities on the cellular levels of individual isoprene PP metabolites and downstream products, as well as to determine whether the observed lower expression level of NUDT18 in cancerous cells is associated with the activity of NUDT18 with isoprene PPs.

In conclusion, we here present a novel and pronounced activity of human NUDT15 and NUDT18 in catalyzing the hydrolysis of isoprene PPs. This discovery suggests a potential role for these enzymes in isoprenoid metabolism in animals.

## Materials and methods

### Protein production

The human NUDIX enzymes MTH1 (NUDT1, P36639), NUDT2 (P50583), NUDT3 (O95989), NUDT4 (Q9NZJ9), NUDT7 (P0C024), NUDT9 (Q9BW91), NUDT10 (Q9BW91), NUDT11 (Q96G61), NUDT12 (Q9BQG2), NUDT14 (O95848), NUDT15 (Q9NV35), NUDT16 (Q96DE0), NUDT17 (P0C025), NUDT18 (Q6ZVK8), NUDT21 (Q69YN4), and NUDT22 (Q9BRQ3) were produced as described previously [20]. The UniProt IDs for each protein are shown in parentheses. In brief, NUDIX enzymes were expressed in *E. coli* as N-terminally His-tagged proteins and purified using His-Trap HP followed by gel filtration or cation exchange chromatography. NUDT15His49Ala cDNA was purchased from (GeneArt, Regensburg, Germany) and subcloned into pNIC28 (a kind gift from PSF, Karolinska Institutet) using NdeI and SalI. NUDT15His49A was expressed in BL21 (DE3) T1R pRARE2 at 18 °C overnight after induction with 0.5 mM IPTG. The sonicated lysate was centrifuged, filtered, and purified using His-Trap HP (GE Healthcare, Freiburg, Baden-Württemberg, Germany) followed by gel filtration using HiLoad 16/60 Superdex 75 columns on an ÄKTA Xpress. The purity of purified proteins was assessed using SDS/PAGE analysis. Proteins were stored in storage buffer (20 mM HEPES, 300 mM NaCl, 10% glycerol, 2 mM TCEP, pH 7.5) and kept as aliquots at −80 °C.

### Screening of NUDIX enzymes for activity with isoprene PPs

Hydrolysis activity of a panel of 17 human NUDIX proteins with DMAPP (Sigma-Aldrich, Saint Louis, MO, USA, #D4287) and IPPP (Sigma-Aldrich, #I0503) was tested by incubating 100 μM of each isoprene PP with

100 nM human NUDIX enzyme for 30 min at 22 °C. Formed Pi was detected by the addition of Malachite green reagent [47] followed by measurement of absorbance at 630 nm, after incubation at 22 °C for 15 min. This experiment was performed once with data points in triplicate due to the limited availability of some of the NUDIX enzymes. The activity of NUDT15 and NUDT18 (100 nM) was retested with 100 μM IPPP and DMAPP and also tested with 100 μM Mevalonate pyrophosphate (MPP, Sigma-Aldrich, #94259), Geranyl-PP (GPP, Sigma-Aldrich, #G6772), Farnesyl-PP, (FPP, Sigma-Aldrich, #F6892), and GGPP (Sigma-Aldrich, #G6025) in assay buffer (100 mM tris acetate pH 8.0, 40 mM NaCl, 10 mM magnesium acetate, and 0.01% Tween 20) and compared to the activity with 100 μM of the previously identified substrates dGTP (GE Healthcare, #27-1870-04) for NUDT15 and 8-oxo-dGDP (Jena Bioscience, Jena, Germany, NU-1158) for NUDT18. In addition, since NUDT15 is closely related to MutT homolog 1 (MTH1, NUDT1) the activity of 50 nM *E. coli* MutT (P08337) with 100 μM GPP as well as with 100 μM dGTP as a control was tested as described above.

### LC–MS analysis of NUDT15 and NUDT18 catalyzed GPP and FPP hydrolysis products

1 mM GPP was incubated with 0.5 μM NUDT18 or 1 μM NUDT15 in reaction buffer (0.1 M tris acetate pH 8.0, 40 mM NaCl, 10 mM Magnesium acetate) at 22 °C with rotation. The reaction was stopped at different time points, ranging from 0 to 180 min for NUDT18 and 0 to 120 min for NUDT15, by removing an aliquot to which EDTA was added (90 mM final concentration) in order to chelate Mg<sup>2+</sup> ions needed for catalysis. The samples were then heated for 5 min at 75 °C to denature the enzyme, followed by centrifugation at 17 000 g for 10 min to precipitate the denatured protein. The supernatants were analyzed using an (Agilent, Clara, California, USA) 1100 HPLC system equipped with an X-bridge C18 column 5 μM (3 × 50 mm) coupled to an Agilent MSD mass spectrometer. For analysis of FPP hydrolysis the same procedure was used with the modification that 0.5 mM FPP was incubated with 10 μM NUDT15 or NUDT18 and samples were taken at various time points between 0 and 225 min, and then prepared and analyzed as described above for the analysis of GPP hydrolysis.

### Detailed kinetic analysis of NUDT15 and NUDT18 with isoprene PPs

To further analyze the activity of NUDT18 and NUDT15 with isoprene PPs a detailed kinetic characterization was performed with a panel of isoprene PPs. Initial rates were determined using 25 nM of NUDT18 and substrate concentrations ranging from 0 to 50 μM for GPP and 0–100 μM for MPP, DMAPP, IPPP, FPP, and GGPP. For saturation

curves produced with NUDT15 25 nM enzyme was used and substrate concentration ranges used were as follows: 0–50  $\mu\text{M}$  for GPP, 0–200  $\mu\text{M}$  for DMAPP, and 0–150  $\mu\text{M}$  for IPPP. Activities were assayed in reaction buffer (100 mM Tris acetate pH 8.0, 40 mM NaCl, 10 mM magnesium acetate, and 0.01% Tween 20). Reactions were stopped after 10, 20, and 30 min incubation time at 22 °C and inorganic phosphate (Pi), released upon hydrolysis, was detected by the addition of malachite green reagent and measurement of the absorbance at 630 nm using a Hidex plate reader. A Pi standard curve on the assay plates was used to convert absorbance to amount of Pi produced. Initial rates were determined in duplicate and saturation curve experiments were performed twice apart from for NUDT15 activity with FPP and GGPP which only was performed once due to the poor activity. Kinetic parameters were determined by fitting the Michaelis–Menten equation to initial rate data using (GRAPHPAD PRISM, Boston, MA, USA) 8.0.

### Activity analysis of NUDT15wt, NUDT15H49A, and MutT with dGTP and GPP

Activity with 100  $\mu\text{M}$  GPP was assayed in assay buffer (0.1 M Tris acetate pH 8.0, 40 mM NaCl, 10 mM magnesium acetate, and 0.01% Tween20) using 100 nM NUDT15H49A, NUDT15WT, or MutT. Activity with 100  $\mu\text{M}$  dGTP was monitored in assay buffer fortified with PPase 0.4 U·mL<sup>-1</sup>, converting PPi to Pi, and 50 nM NUDT15H49A, 5 nM NUDT15WT, or 50 nM MutT. Formed Pi was detected after incubation for 30 min at 22 °C by the addition of Malachite green reagent. A Pi standard curve was used to calculate the concentration of produced Pi. Saturation curves of NUDT15WT and NUDT15H49A were produced by determining initial rates in assay buffer (0.1 M Tris acetate pH 8.0, 40 mM NaCl, and 10 mM magnesium acetate) using 50 nM NUDT15 WT or 100 nM NUDT15H49A and substrate concentrations of GPP ranging from 0 to 200  $\mu\text{M}$ . Initial rates were determined in duplicate. For saturation curves with dGTP, dGTP was varied between 0 and 400  $\mu\text{M}$ , and initial rates of 5 nM NUDT15WT and 50 nM NUDT15H49A were monitored.

### Crystallization and structure determination of the NUDT15-GP complex

Purified human NUDT15 (20 mg·mL<sup>-1</sup>) was preincubated with 10 mM GPP (Sigma-Aldrich) for 2 h at 20 °C. The protein was crystallized using sitting drop vapor diffusion at 20 °C in 0.1 M Tris–HCl pH 8.5, 0.2 M sodium acetate, and 30% PEG4000. Protein crystals were flash-frozen directly in liquid nitrogen without adding additional cryoprotectant. X-ray diffraction data were collected at station I03 of the Diamond Light Source (Oxford, UK) equipped with a PILATUS-6M detector. A complete dataset was collected on a single crystal at 100 K. The dataset was

processed and scaled with DIALS [48] and AIMLESS [49] within the CCP4 SUITE [50]. Molecular replacement was performed in PHASER [51], using a human NUDT15 structure (PDB: 5LPG) with all ligands and waters removed. Several rounds of manual model building and refinement were performed using COOT [52] and REFMAC5 [53] during which water and the ligand GP were added to the structure. Data processing and refinement statistics are listed in Table 3. The coordinates and structure factors for the NUDT15-GP structure presented in this paper were deposited in the PDB database (PDB: 7R0D).

### NUDT18 expression analysis

NUDT18 expression data from 1408 cell lines were downloaded from the DepMap database (<https://depmap.org/>). Analysis of variance (ANOVA) was applied to identify the presence of differences in gene expression between cell lines originating from different tissues. A Tukey *post hoc* test was performed to identify significant differences.

### Acknowledgements

We thank Athina Pliakou, Louise Sjöholm, Kristina Edfeldt, Mari Kullman Magnusson, Flor Pineiro, and Sabina Eriksson for their assistance in the Helleday Lab. We thank Dr Niklas Schultz for scientific input. We thank the beamline scientists at Diamond Light Source (United Kingdom, proposal mx21625) for their support in structural biology data collection. We are grateful to the Protein Science Facility at Karolinska Institutet/SciLifeLab (<http://ki.se/psf>) for help with protein production. This work was supported by grants from the Swedish Research Council (2022-03681 to PS, 2015-00162 and 2017-06095 to TH), the Swedish Cancer Society (20 1287 PjF to PS and 21 1490 Pj to TH), the European Research Council (ERC-AdG-TAROX-695376 to TH), the Knut and Alice Wallenberg Foundation (KAW2014.0273 to TH and 2022-0209 to VT), Torsten and Ragnar Söderberg Foundation (to TH), the Helleday Foundation (to JEU), The Swedish Foundation for Strategic Research (UKR22-0035 to VT), and KI funds (2020-02211 to A-SJ).

### Conflict of interest

The authors declare no conflict of interest.

### Author contributions

A-SJ wrote the manuscript with input from ERS and PS. All authors commented on the manuscript. A-SJ

and PS conceived the project. A-SJ designed, performed, and analyzed all biochemical experiments. DK, JEU, and IA produced and analyzed proteins. TK and KSV performed the LC-MS analysis. Protein structure was solved by ERS and PS. ERS performed structural analyses. VT performed gene expression analyses. A-SJ, PS, and TH supervised the project and acquired funding.

## Peer review

The peer review history for this article is available at <https://www.webofscience.com/api/gateway/wos/peer-review/10.1111/febs.17202>.

## Data availability statement

All data can be shared upon request made to the corresponding author. Crystal structure data are deposited in PDB: [7R0D](https://www.rcsb.org/structure/7R0D).

## References

- Holstein SA & Hohl RJ (2004) Isoprenoids: remarkable diversity of form and function. *Lipids* **39**, 293–309.
- Goldstein JL & Brown MS (1990) Regulation of the mevalonate pathway. *Nature* **343**, 425–430.
- Nguyen UT, Guo Z, Delon C, Wu Y, Deraeve C, Franzel B, Bon RS, Blankenfeldt W, Goody RS, Waldmann H *et al.* (2009) Analysis of the eukaryotic prenylome by isoprenoid affinity tagging. *Nat Chem Biol* **5**, 227–235.
- Kho Y, Kim SC, Jiang C, Barma D, Kwon SW, Cheng J, Jaunbergs J, Weinbaum C, Tamanoi F, Falck J *et al.* (2004) A tagging-via-substrate technology for detection and proteomics of farnesylated proteins. *Proc Natl Acad Sci USA* **101**, 12479–12484.
- Takai Y, Sasaki T & Matozaki T (2001) Small GTP-binding proteins. *Physiol Rev* **81**, 153–208.
- Politiek FAA & Waterham HRR (2021) Compromised protein prenylation as pathogenic mechanism in mevalonate kinase deficiency. *Front Immunol* **12**, 724991.
- Buhaescu I & Izzedine H (2007) Mevalonate pathway: a review of clinical and therapeutical implications. *Clin Biochem* **40**, 575–584.
- Frenkel J, Rijkers GT, Mandey SH, Buurman SW, Houten SM, Wanders RJ, Waterham HR & Kuis W (2002) Lack of isoprenoid products raises ex vivo interleukin-1beta secretion in hyperimmunoglobulinemia D and periodic fever syndrome. *Arthritis Rheum* **46**, 2794–2803.
- Liao JK & Laufs U (2005) Pleiotropic effects of statins. *Annu Rev Pharmacol Toxicol* **45**, 89–118.
- Kaneko R, Tsuji N, Asanuma K, Tanabe H, Kobayashi D & Watanabe N (2007) Survivin down-regulation plays a crucial role in 3-hydroxy-3-methylglutaryl coenzyme a reductase inhibitor-induced apoptosis in cancer. *J Biol Chem* **282**, 19273–19281.
- Hinson DD, Chambliss KL, Toth MJ, Tanaka RD & Gibson KM (1997) Post-translational regulation of mevalonate kinase by intermediates of the cholesterol and nonsterol isoprene biosynthetic pathways. *J Lipid Res* **38**, 2216–2223.
- Schumacher MM, Elsabrouty R, Seemann J, Jo Y & DeBose-Boyd RA (2015) The prenyltransferase UBIAD1 is the target of geranylgeraniol in degradation of HMG CoA reductase. *Elife* **4**, e05560.
- Crespo R, Villegas SM, Abba MC, de Bravo MG & Polo MP (2013) Transcriptional and posttranscriptional inhibition of HMGCR and PC biosynthesis by geraniol in 2 hep-G2 cell proliferation linked pathways. *Biochem Cell Biol* **91**, 131–139.
- Polo MP & de Bravo MG (2006) Effect of geraniol on fatty-acid and mevalonate metabolism in the human hepatoma cell line hep G2. *Biochem Cell Biol* **84**, 102–111.
- Meigs TE, Roseman DS & Simoni RD (1996) Regulation of 3-hydroxy-3-methylglutaryl-coenzyme a reductase degradation by the nonsterol mevalonate metabolite farnesol in vivo. *J Biol Chem* **271**, 7916–7922.
- Meigs TE & Simoni RD (1997) Farnesol as a regulator of HMG-CoA reductase degradation: characterization and role of farnesyl pyrophosphatase. *Arch Biochem Biophys* **345**, 1–9.
- Fukunaga K, Arita M, Takahashi M, Morris AJ, Pfeffer M & Levy BD (2006) Identification and functional characterization of a presqualene diphosphate phosphatase. *J Biol Chem* **281**, 9490–9497.
- Miriyala S, Subramanian T, Panchatcharam M, Ren H, McDermott MI, Sunkara M, Drennan T, Smyth SS, Spielmann HP & Morris AJ (2010) Functional characterization of the atypical integral membrane lipid phosphatase PDP1/PPAPDC2 identifies a pathway for interconversion of isoprenols and isoprenoid phosphates in mammalian cells. *J Biol Chem* **285**, 13918–13929.
- Mildvan AS, Xia Z, Azurmendi HF, Saraswat V, Legler PM, Massiah MA, Gabelli SB, Bianchet MA, Kang LW & Amzel LM (2005) Structures and mechanisms of Nudix hydrolases. *Arch Biochem Biophys* **433**, 129–143.
- Carreras-Puigvert J, Zitnik M, Jemth AS, Carter M, Unterlass JE, Hallstrom B, Loseva O, Karem Z, Calderon-Montano JM, Lindskog C *et al.* (2017) A comprehensive structural, biochemical and biological profiling of the human NUDIX hydrolase family. *Nat Commun* **8**, 1541.

- 21 McLennan AG (2006) The Nudix hydrolase superfamily. *Cell Mol Life Sci* **63**, 123–143.
- 22 Magnard JL, Rocchia A, Caissard JC, Vergne P, Sun P, Hecquet R, Dubois A, Hibrand-Saint Oyant L, Jullien F, Nicole F *et al.* (2015) PLANT VOLATILES. Biosynthesis of monoterpene scent compounds in roses. *Science* **349**, 81–83.
- 23 Liu J, Guan Z, Liu H, Qi L, Zhang D, Zou T & Yin P (2018) Structural insights into the substrate recognition mechanism of Arabidopsis GPP-bound NUDX1 for noncanonical monoterpene biosynthesis. *Mol Plant* **11**, 218–221.
- 24 Jemth AS, Scaletti ER, Homan E, Stenmark P, Helleday T & Michel M (2022) Nudix hydrolase 18 catalyzes the hydrolysis of active triphosphate metabolites of the antivirals remdesivir, ribavirin, and molnupiravir. *J Biol Chem* **298**, 102169.
- 25 Carter M, Jemth AS, Hagenkort A, Page BD, Gustafsson R, Griese JJ, Gad H, Valerie NC, Desroses M, Bostrom J *et al.* (2015) Crystal structure, biochemical and cellular activities demonstrate separate functions of MTH1 and MTH2. *Nat Commun* **6**, 7871.
- 26 Henry LK, Thomas ST, Widhalm JR, Lynch JH, Davis TC, Kessler SA, Bohlmann J, Noel JP & Dudareva N (2018) Contribution of isopentenyl phosphate to plant terpenoid metabolism. *Nat Plants* **4**, 721–729.
- 27 Takagi Y, Setoyama D, Ito R, Kamiya H, Yamagata Y & Sekiguchi M (2012) Human MTH3 (NUDT18) protein hydrolyzes oxidized forms of guanosine and deoxyguanosine diphosphates: comparison with MTH1 and MTH2. *J Biol Chem* **287**, 21541–21549.
- 28 Hashiguchi K, Hayashi M, Sekiguchi M & Umezaki K (2018) The roles of human MTH1, MTH2 and MTH3 proteins in maintaining genome stability under oxidative stress. *Mutat Res* **808**, 10–19.
- 29 Cai JP, Ishibashi T, Takagi Y, Hayakawa H & Sekiguchi M (2003) Mouse MTH2 protein which prevents mutations caused by 8-oxoguanine nucleotides. *Biochem Biophys Res Commun* **305**, 1073–1077.
- 30 Nishii R, Mizuno T, Rehling D, Smith C, Clark BL, Zhao XJ, Brown SA, Smart B, Moriyama T, Yamada Y *et al.* (2021) NUDT15 polymorphism influences the metabolism and therapeutic effects of acyclovir and ganciclovir. *Nat Commun* **12**, 4181.
- 31 Zhang SM, Rehling D, Jemth AS, Throup A, Landazuri N, Almlof I, Gottmann M, Valerie NCK, Borhade SR, Wakchaure P *et al.* (2021) NUDT15-mediated hydrolysis limits the efficacy of anti-HCMV drug ganciclovir. *Cell Chem Biol* **28**, 1693–1702.e6.
- 32 Valerie NC, Hagenkort A, Page BD, Masuyer G, Rehling D, Carter M, Bevc L, Herr P, Homan E, Sheppard NG *et al.* (2016) NUDT15 hydrolyzes 6-Thio-DeoxyGTP to mediate the anticancer efficacy of 6-thioguanine. *Cancer Res* **76**, 5501–5511.
- 33 Moriyama T, Nishii R, Perez-Andreu V, Yang WJ, Klussmann FA, Zhao XJ, Lin TN, Hoshitsuki K, Nersting J, Kihira K *et al.* (2016) NUDT15 polymorphisms alter thiopurine metabolism and hematopoietic toxicity. *Nat Genet* **48**, 367–373.
- 34 Kavanagh KL, Dunford JE, Bunkoczi G, Russell RGG & Oppermann U (2006) The crystal structure of human geranylgeranyl pyrophosphate synthase reveals a novel hexameric arrangement and inhibitory product binding. *J Biol Chem* **281**, 22004–22012.
- 35 Kavanagh KL, Guo K, Dunford JE, Wu X, Knapp S, Ebetino FH, Rogers MJ, Russell RG & Oppermann U (2006) The molecular mechanism of nitrogen-containing bisphosphonates as antiosteoporosis drugs. *Proc Natl Acad Sci USA* **103**, 7829–7834.
- 36 Bar-Even A, Noor E, Savir Y, Liebermeister W, Davidi D, Tawfik DS & Milo R (2011) The moderately efficient enzyme: evolutionary and physicochemical trends shaping enzyme parameters. *Biochemistry* **50**, 4402–4410.
- 37 Schumacher MM, Jun DJ, Johnson BM & DeBose-Boyd RA (2018) UbiA prenyltransferase domain-containing protein-1 modulates HMG-CoA reductase degradation to coordinate synthesis of sterol and nonsterol isoprenoids. *J Biol Chem* **293**, 312–323.
- 38 Crespo R, Montero Villegas S, Abba MC, de Bravo MG & Polo MP (2013) Transcriptional and posttranscriptional inhibition of HMGCR and PC biosynthesis by geraniol in 2 hep-G2 cell proliferation linked pathways. *Biochem Cell Biol* **91**, 131–139.
- 39 Huang Y, Yang XL, Ni YH & Xu ZM (2018) Geraniol suppresses proinflammatory mediators in phorbol 12-myristate 13-acetate with A23187-induced HMC-1 cells. *Drug Des Devel Ther* **12**, 2897–2903.
- 40 Kim J, Lee JN, Ye J, Hao R, DeBose-Boyd R & Ye J (2013) Sufficient production of geranylgeraniol is required to maintain endotoxin tolerance in macrophages. *J Lipid Res* **54**, 3430–3437.
- 41 Forman BM, Goode E, Chen J, Oro AE, Bradley DJ, Perlmann T, Noonan DJ, Burka LT, McMorris T, Lamph WW *et al.* (1995) Identification of a nuclear receptor that is activated by Farnesol metabolites. *Cell* **81**, 687–693.
- 42 Dhar MK, Koul A & Kaul S (2013) Farnesyl pyrophosphate synthase: a key enzyme in isoprenoid biosynthetic pathway and potential molecular target for drug development. *N Biotechnol* **30**, 114–123.
- 43 Hogenboom S, Tuyp JJM, Espeel M, Koster J, Wanders RJA & Waterham HR (2004) Phosphomevalonate kinase is a cytosolic protein in humans. *J Lipid Res* **45**, 697–705.
- 44 Ownby SE & Hohl RJ (2003) Isoprenoid alcohols restore protein isoprenylation in a time-dependent manner independent of protein synthesis. *Lipids* **38**, 751–759.

- 45 Rehling D, Zhang SM, Jemth A-S, Koolmeister T, Throup A, Wallner O, Scaletti E, Moriyama T, Nishii R & Davies J (2021) Crystal structures of NUDT15 variants enabled by a potent inhibitor reveal the structural basis for thiopurine sensitivity. *J Biol Chem* **296**, 100568.
- 46 Moriyama T, Yang YL, Nishii R, Ariffin H, Liu CC, Lin TN, Yang WJ, Lin DT, Yu CH, Kham S *et al.* (2017) Novel variants in NUDT15 and thiopurine intolerance in children with acute lymphoblastic leukemia from diverse ancestry. *Blood* **130**, 1209–1212.
- 47 Baykov AA, Evtushenko OA & Avaeva SM (1988) A malachite green procedure for orthophosphate determination and its use in alkaline phosphatase-based enzyme immunoassay. *Anal Biochem* **171**, 266–270.
- 48 Parkhurst JM, Winter G, Waterman DG, Fuentes-Montero L, Gildea RJ, Murshudov GN & Evans G (2016) Robust background modelling in DIALS. *J Appl Cryst* **49**, 1912–1921.
- 49 Evans P (2006) Scaling and assessment of data quality. *Acta Crystallogr D* **62**, 72–82.
- 50 Bailey S (1994) The Ccp4 suite – programs for protein crystallography. *Acta Crystallogr D* **50**, 760–763.
- 51 McCoy AJ, Grosse-Kunstleve RW, Adams PD, Winn MD, Storoni LC & Read RJ (2007) Phaser crystallographic software. *J Appl Cryst* **40**, 658–674.
- 52 Emsley P & Cowtan K (2004) COOT: model-building tools for molecular graphics. *Acta Crystallogr D* **60**, 2126–2132.
- 53 Murshudov GN, Vagin AA & Dodson EJ (1997) Refinement of macromolecular structures by the maximum-likelihood method. *Acta Crystallogr D* **53**, 240–255.